GEOPOTENTIAL HEIGHT PATTERNS AT 500MB ASSOCIATED WITH MAJOR DUST STORMS IN THE UNITED STATES/MEXICO BORDER REGION DURING JANUARY-MAY OF 2011-2014

By

Rebecca Britt Armenta

A thesis submitted to the Graduate School
in partial fulfillment of the requirements
for the degree
MASTER OF SCIENCE

Major Subject: Plant & Environment Science

New Mexico State University
Las Cruces, New Mexico
May 2016

“Geopotential Height Patterns At 500mb Associated With Major Dust Storms In The United States/Mexico Border Region During January-May of 2011-2014,” a thesis prepared by Rebecca Britt Armenta in partial fulfillment of the requirements for the degree Master of Science, has been approved and accepted by the following:

Loui Reyes
Dean of the Graduate School

David W. DuBois
Chair of the Examining Committee

Date

Committee in charge:

Dr. David W. DuBois, Chair

Dr. April L. Ulery

Dr. Soumaila Sanogo

ACKNOWLEDGEMENT

The NCEP Reanalysis data was provided by the NOAA/OAR/ESRL PSD, Boulder, Colorado, USA, from their Web site at http://www.esrl.noaa.gov/psd/.

This research was supported by the following grants and organizations: 2011 Unidata Equipment Grant (Unidata UCAR sub-award No. Z11-90984); NM Dept. of Health, Office of Border Health (FY16 MOA #19165, FY15 MOA #18137, FY14 MOA #16871, FY13 MOA #15218); NM Environment Department, Air Quality Bureau (New Mexico Environment Department MOU #13-667-3000-0004); Climate Assessment for the Southwest (CLIMAS) (CLIMAS prime award NA12OAR4310124, sub-award 100755); the NM State Climate Office and the New Mexico State University College of Agriculture Consumer and Environmental Sciences' Agricultural Experiment Station.

For invaluable help with the statistical analysis I thank Samantha Johnson of Rice University who was here during the summer of 2015 assisting Professor Steve Thomas of NMSU, Professor Dawn VanLeeuwen, and Professor Naomi Schmidt, both from the Economics, Applied Statistics & International Business Department at NMSU. I would like to thank Ms. Annette Walker from the US Navy Research Laboratory in Monterey, CA for many useful discussions and guidance in this work.

I would like to express my gratitude to Dr. David W. DuBois for giving me the opportunity to work under his mentorship. I want to thank my co-advisor, Max P. Bleiweiss, without whom none of this could have happened, for his support and valuable ideas and for his advice in the remote sensing lab. I want to thank the two other members of my graduate committee, Dr. April L. Ulery and Dr. Soumaila Sanogo. Their guidance and support has been invaluable. To the people in Dr. DuBois's group: thank you for your friendship. To the people in Max P. Bleiweiss' group; and, especially Miranda Flores and Merrill Bean for their time and expertise on the development of this project. I extend deepest love and admiration, to my son (Alexander A. Acuna), my mother (Lucema Armenta), and my sister (Adriana H. B. Armenta); thank you for always being there for me. Finally, I would like to acknowledge the department of Plant and Environmental Sciences at the New Mexico State University.

VITA

Born 1987	El Paso, Texas
2006	Graduated from Coronado High School El Paso, Texas
2011	Graduated from the University of Texas at El Paso El Paso, Texas
2011-2016	Research Assistant, Plant and Environmental Science New Mexico State University

Professional and Honorary Societies

American Geophysical Union

Field of Study

Major Field: Plant and Environmental Science

ABSTRACT

GEOPOTENTIAL HEIGHT PATTERNS AT 500MB ASSOCIATED WITH MAJOR DUST STORMS IN THE UNITED STATES/MEXICO BORDER REGION DURING JANUARY-MAY OF 2011-2014

BY

REBECCA BRITT ARMENTA, B.S.

New Mexico State University

Las Cruces, New Mexico, 2016

Dr. David W. DuBois, Chair

Dust storms affect the environment, health, and economy of a region. Therefore, it is important to understand the main causes and sources of windblown dust. To help understand the causes of the dust storms in the border region of the Southwestern US, the synoptic scale meteorological conditions present at the time of approximately 60 dust storm events from 2011 through 2014 (from about 600 dust events over a 15 year period) have been studied. From that, particular “synoptic scale” geopotential height patterns for dust events in the border region have been identified. To do this, the North American Regional Reanalysis (NARR) 500mb geopotential height patterns at 18 GMT was used to investigate whether the "observational" experience agrees with the hypothesis that a key 500mb geopotential height low pressure pattern exists in the Great Basin of the Southwestern US at the time the dust storm begins. In this analysis, individual 500mb geopotential height patterns were compared to a mean dust day 500mb geopotential height pattern (the key). To do this comparison, a tool from image analysis that measures the similarities between two images was used. This tool is the image cross-correlation function and is similar to the Pearson product-moment correlation. For each of the 4 years studied, the cross-correlation between dust day pressure patterns and the key as well as the cross-correlation between non-dust day pressure patterns and the key were obtained. To determine whether there is a difference between the cross-correlations derived with dust day pressure patterns and those obtained from non-dust day pressure patterns, a statistical analysis based on the Wilcoxon Rank Sum test was used to compare the distributions of dust day and non-dust day correlation results. Results show that there is a significant difference between distributions ($P < 0.0002$). This means that there is a particular low pressure feature northwest of the NM/Mexico border at 18 GMT at the time the dust storm begins; and, that no such feature is present during non-dust days. This cross-correlation technique can therefore be used to develop a tool for use by a forecaster as well as for creating a climatology of dust events in the border region of the Southwestern US over a ~35 year period (from the NARR archive).

TABLE OF CONTENTS

LIST OF TABLES

LIST OF FIGURES

ACRONYMS AND ABBREVIATIONS

°C: degree Celsius
BT: Brightness Temperature
ca.: Circa
CA: California
CARSAME: Center for Applied Remote Sensing In Agriculture, Meteorology and Environment
CLIMAS: Climate Assessment for the Southwest
ENVI: Environment for Visualizing Images
ESRL PSD: Earth System Research Laboratory Physical Sciences Division
ETC: Extratropical Cyclone
FY: Fiscal Year
GFS: Global Forecast System
GMT: Greenwich Mean Time
GOES: Geostationary Operational Environmental Satellite
hPa: hectopascal
J: joule
K: kelvin
kg: kilogram
km: kilometer
mb: millibar
mm/dd: Month/Day
MOA: Memorandum of Agreement
NAM: North America Mesoscale Forecast System
NARR: North American Regional Reanalysis
NCEP: National Center for Environmental Prediction
NM: New Mexico
NMED: New Mexico Environment Department
NMSU: New Mexico State University
NOAA OAR: National Oceanic Atmospheric Administration Office of Oceanic and Atmospheric Research
Pr: Probability
P-value: Probability Value
RAMMB: Regional and Mesoscale Meteorology Branch
SAS: Statistical Analysis System
SHP: Southern High Plains
SOP: Standard Operating Procedure
SW: Southwest/Southwestern
TX: Texas
UCAR: University Corporation for Atmosphere Research
US: United States

1.0 INTRODUCTION

During the past 15 years, researchers at New Mexico State University have been collecting data on regional dust storms. During this time, approximately 500-600 days have been observed to produce a dust storm in the region encompassed by 20-45 degrees north latitude, 90-120 degrees west longitude. Even though some of these data have been used in prior limited studies (e.g., Rivera-Rivera et al., 2009), there has been no extensive analysis of these data and the meteorological processes that cause the dust events to occur. That is the focus of this research. In order to understand the macroscale processes that create dust storms, the atmospheric dynamics, at the synoptic scale, present at the time of dust storm initiation, must be identified. This will allow an understanding of the climatological influences on dust storm development (Goudie, 2009; Al-Dousari and Al-Awadhi, 2012; Ganor, et al., 2010). There have been few studies in identifying and classifying local smaller dust storms in regions affected by drought and/or regions that are naturally arid/semi-arid. These local events have been reported to impact directly on human health (Kavouras et al., 2015; DuBois et al., 2012; Grineski et al., 2011; Kolivras et al., 2001; Hector et al., 2011; and Rodopoulou et al., 2014), and transportation (Ashley et al., 2015; Patterson and Gillette, 1977; Burritt and Hyers, 1981, and Brazel and Hsu, 1981) (e.g., when low visibility is reported along main highways) and air quality (Hall, 1981 and Gertler et al., 1995; Kavouras et al., 2009; Chow et al., 1999).

Information on local dust storm development is needed in areas such as the Southwestern United States, Northern Chihuahua, and West Texas where dust storms create hazardous conditions. It is understood that the dust storms originate from a region where loose soils are available for saltation and strong winds can occur. Characterization of the geography of the region is necessary to better understand those places where it is more likely that certain soils may be available for dust storm emission. The synoptic meteorological conditions that influence a dust storm also needs to be studied so that the results of this study may be used to develop forecast tools to help mitigate the effects of dust storms. Our study area (SW US/Mexico border region with emphasis on that part of the region along the NM/Mexico border) is also a region where the soils tend to be sandy and friable with sparse vegetation and low rainfall so that gusty winds can cause high levels of dust emissions to occur (Rivera-Rivera et al., 2009 and Lee et al., 2012). The condition of the land surface is of paramount importance to the land's ability to influence the lofting of dust particles into the atmosphere.

A limitation of this investigation lies with the constraints imposed by the Geostationary Operational Environmental Satellite (GOES) imagery that allows for the identification only of larger dust plumes because the GOES imager is 4km spatial resolution and the GOES sounder is 10km spatial resolution. It is primarily the GOES imagery that has been used to recognize the presence of a dust event. Therefore, dust events from convective activity or those that are due to more localized winds are missed. Smaller and short-lived dust events as well as those occurring beneath the cloud cover will not be recorded in this archive. Events may have also been missed because of inattention to existing conditions. In order that there is a more complete understanding of the adverse effects of dust storms and the associated meteorological conditions, previous research on these issues will now be reviewed. Additional details regarding the method used to locate the source of the dust storm plumes are given in Appendix A.

Investigation of previous research on synoptic scale meteorological conditions during dust storm events in the Southwestern US as well as elsewhere in the world will allow a more complete picture of the possible dynamics to appear. Orgill and Sehmel (1976) summarized the 6 major meteorological conditions that lead to major dust events with convective systems being first. Following that are warm and cold frontal passages and cyclogenesis; both of these are the causes of the dust events catalogued in our region. In addition, Orgill and Sehmel (1976) stated that the event frequency peaks in the early and late spring months; again, as confirmed in our data archive and discussed by others (e.g., Novlan et al., 2007). They also presented maps of frequency of dust hours; both annually and by month for the period between 1940 and 1970 based on weather station data. According to these maps, the greatest number of dust hours occurs in the western states. The largest number of hours is in the Great Plains and Southern Great Plains followed by New Mexico and Southern California and Arizona.

Knippertz (2014) lists four meteorological conditions that cause the emission of dust. These are monsoon-type flows, synoptic-scale systems such as cyclones and their associated fronts, gust fronts from convective systems, and intense dry convection. In our region and for the types of dust events which are considered, it is the cyclone and its associated cold front that is of interest.

Indeed, in other regions of the world, it has been recognized that the extratropical cyclone (ETC) and associated cold front is the synoptic weather pattern responsible for the dust storm initiation and development. In fact, in general, the ETCs are responsible for the weather systems and resulting climate experienced at mid-latitudes (Pinto et al., 2005). In the Gobi Desert, severe dust storms are caused in a large part by spring cyclones that develop over the Mongolian Plateau (Adachi, 2007). . In addition, the cold front and squall line associated with the cyclone are the location of the intense winds (Zhao and Zhao, 2006). In an overview of dust storms in China, Wang et al. (2004) stated that the arid and the semi-arid regions of China are from where the dust storms originate. They also indicated that most of the 43 spring dust storms near Beijing between 1991 and 2002 were closely related to cyclone occurrence. Furthermore, Wang et al. (2004) stated that the dust storm process is very complicated and additional information beyond the existence of the spring cyclone, such as vegetation cover and soil moisture or antecedent precipitation, among others, is needed.

In Israel, Offer and Goossens (2001) studied the most severe dust storms in the Northern Negev, which are preceded by a pressure drop that is a signal from an approaching cyclone and associated front that supplies the winds necessary for the dust storm to occur: “it is the most common type of dust storm in the Northern Negev”. In Africa, Karam et al. (2010) investigated a particular dust event associated with a Sharav cyclone (a particular type of African cyclone). They stated that dust emission is shown to increase as strong winds associated with cold front passage increase as the cyclone further develops. Overall, they concluded that the cyclone and associated cold front was the major cause of this particular dust storm.

The synoptic scale dynamics during dust storm events in Australia seem to be much different from what is experienced in North America as much of the controlling pressure patterns appear to be dominated by high pressure at the surface that control the overall circulation patterns (Ekström et al., 2004). However, the disturbances that cause the highest frequency of dust events during the Australian spring and summer are associated with cold fronts. Also in Australia, Leslie and Speer (2006) are mainly concerned with modelling dust transport; however, in evaluating their model, they considered three case studies of long-range transport of dust from major dust events. For all three of these cases, they described the synoptic scale meteorology as consisting of surface cold fronts that are associated with tropospheric troughs which may, or may not be well defined low pressure systems.

Closer to the border region of the Southwestern US, some early work on understanding dust storms in Arizona was conducted (Brazel and Nickling, 1986 and Nickling and Brazel, 1984). The most common weather type associated with dust storms in Arizona is the frontal passage that accounts for most of the events that happen during late autumn, winter, and spring (Brazel and Nickling, 1986). In an article about Arizona dust storms over a 15 year period (1965-1985), Nickling and Brazel (1984) considered both the spatial and temporal characteristics of dust storms using weather station visibility measurements. Events near Phoenix were more severe than elsewhere in the state, and were attributed to downdrafts from thunderstorms. Nickling and Brazel (1984) also stated that less intense dust storms of longer duration occur during late winter into spring and that those events are associated with cyclones that include cold fronts with cutoff lows. Nickling and Brazel (1984) go on to say that research is also needed to determine surface conditions that influence the emission of dust: “antecedent moisture conditions, surface soil and vegetation conditions, and anthropogenic factors”. Nickling and Brazel (1984) associate local, small scale wind events (such as one might find with dust devils) and the specific surface conditions at the time of the event such as agricultural or construction activity caused many events that are not associated with either thunderstorms or cold fronts.

In a study of Texas/Southern Great Plains dust events, Bernier (1995) states that West Texas dust events occur mostly during December-May and are the result of frontal passages and troughs. During prehistoric times in the Southern High Plains (SHP), that basically extends over about half the panhandle of Texas and into the eastern part of NM, Holliday (1991) describes the SHP as a semiarid, short-grass prairie that was created by “the accumulation of wind-blown sediment” to form a flat, featureless surface that is pock-marked by depressions known as playas and with some relief provided by sand dunes. Analysis of the sediments indicate that deposition has occurred over the last several million years and that although agriculture in the region has affected the impact of erosion, it is not responsible for the process that is generated by the high winds that occur, primarily, in the spring months. Wigner and Peterson (1987) studied the synoptic conditions for blowing dust on the Texas South Plains for the period 1947-1984, in which 1,638 events were noted with ~50% generated by "mixing down from aloft" from troughs, cold frontal passage was responsible for ~30%, and thunderstorms accounted for ~20%. Wigner and Peterson (1987) stated that the "most spectacular" events are associated with "cyclones, cold fronts or thunderstorm outflows". In a recent article by Lee and Gill (2015), they too attribute Dust Bowl dust events to strong cyclones (so-called, "Colorado Cyclones").

Hahnenberger and Nicoll (2012) described both the meteorological conditions and the surface conditions for dust events since the 1930s that affected Salt Lake City. Their results showed that for 379 dust events (since the 1930s), that "mid-level troughs caused 68%" of the 331 events since 1948 and that, with more detailed analysis, determine that "strengthening cyclonic systems" are what is causing the dust events. Hahnenberger and Nicoll (2012) also discussed a seasonal and diurnal pattern for these events: there is a strong March/April component with a diurnal peak in the afternoon and evening (probably due to a temporal lag as the dust is transported north/northwest from the source regions to the south of Salt Lake City).

Synoptic weather systems serve as a starting point in identifying the variables crucial in understanding the dynamics of the formation of a dust storm event. The 500mb pattern that exists on dusty days is one way to portray the overall upper air synoptic pattern that initiates a dust storm provided that all of the other elements are appropriate for dust emission to occur. The upper level trough, when it is west of our region and north of about 32 degrees north, is the pattern in which we are interested. These troughs are associated with jet stream winds. The jet stream winds rotate around the cyclone which allows the winds to move upward in a counter clockwise motion. When the surface temperature inversion breaks, mixing between the surface and the top of the planetary boundary layer occurs. This allows the upper level winds to mix down causing dust emission. The surface cold front associated with the trough is the location of the strongest surface winds. The opposite situation to the cold front passage is the region behind the trough which is more stable and without the high winds (Novlan, 2015).

The way in which the cyclonic structure of the atmosphere is recognized is through investigation of the atmospheric pressure where a cyclone manifests itself as a low pressure system, which exists at all altitudes while the atmospheric pressure at a certain height is lower than the surrounding region. The way in which this information is recorded is by converting the atmospheric pressure to geopotential height, which is the altitude above sea level at which a particular pressure exists. In particular, the levels at which the 500mb pressure exists are well suited to identifying the low and high pressure features in the atmosphere – these levels are known as the 500mb geopotential height. Weather forecasters routinely use the 500mb maps to develop forecast and track storm systems. (Additional information on geopotential heights is given in Appendix B.) Based on this review and supporting documentation relating extratropical cyclones to dust storms, the following research question was formulated: is there a particular 500mb geopotential height pattern that occurs at the beginning of a dust storm that forms in the New Mexico/Mexico border Region? To answer this question, a study of dust storms observed to occur in the region during the spring months of 2011-2014 was conducted. The remainder of this thesis will first describe the data that were used and then the methodology of data analysis that was followed. The results are then presented and discussed after which some guidance for future research into this problem is provided.

2.0 DATA AND METHODS

Our data consisted of two parts: dust event locations and start times and a corresponding collection of synoptic weather patterns (500mb geopotential heights) so that we could determine whether a relationship exists between the two. A regional dust storm dataset, which includes the locations of the dust plume sources for the years 2002-2014 and a reanalysis data set of 500mb geopotential heights were considered to investigate the relationship between the two datasets. To allow this relationship to be characterized, a smaller geographic region that is a spatial subset of the dust storm events is used. The criteria that were used to narrow the field of study were determined by the impact of the dust events on transportation along I-10 and air quality issues near the US/Mexico border.

2.1 Data

The North American Regional Reanalysis (NARR) data, from which the 500mb geopotential heights were extracted, covers the time period from 1979 to present times and is described in Mesinger et al. (2006). These particular data are available at 3hr intervals for 29 pressure levels. A climate reanalysis dataset brings together multiple climate model output and climate observations (station observations, satellite data, and weather radar, among others) so that the final output is of higher quality with better spatial and temporal resolution than could be had from any of the individual input data sets. In addition, all of the various data types are brought into gridded file structures that allows for easy manipulation.

Figure 2.1.1 shows an example of the NARR 500mb geopotential height pattern for April 14, 2012 at 18 GMT (a date during which a dust event occurred) -- note the presence of the low pressure feature centered over the Utah/Arizona border (a feature that becomes the “Albuquerque Low” that is a component of the extratropical cyclone that is observed at the surface and is part of the cyclone that is observed at the 500mb height – the 500mb pattern closely follows nearly the same path, as well). This is also a spatial subset (19.65-44.15 degrees north latitude, 95.15-125.75 degrees west longitude) of the original NARR domain that covers all of North America (Mexico, US, Canada) – it was chosen to better focus on our region. Both of the archives of dust events as well as the NARR dataset were obtained from the NMSU Center for Applied Remote Sensing in Agriculture, Meteorology, and Environment (CARSAME) archives.

The dust event database came about because of interest in monitoring dust storm occurrence and progress using satellite remote sensing at the US Army Research Laboratory (White Sands Missile Range, NM) beginning in 1999. At that time, a protocol was developed, and put into place, to watch for and catalog regional dust events as well as to acquire and store collateral information for these events. As a result of this effort, during the period to 2000 to 2015, approximately 600 days with regional dust storms have been observed (Bleiweiss, 2015).

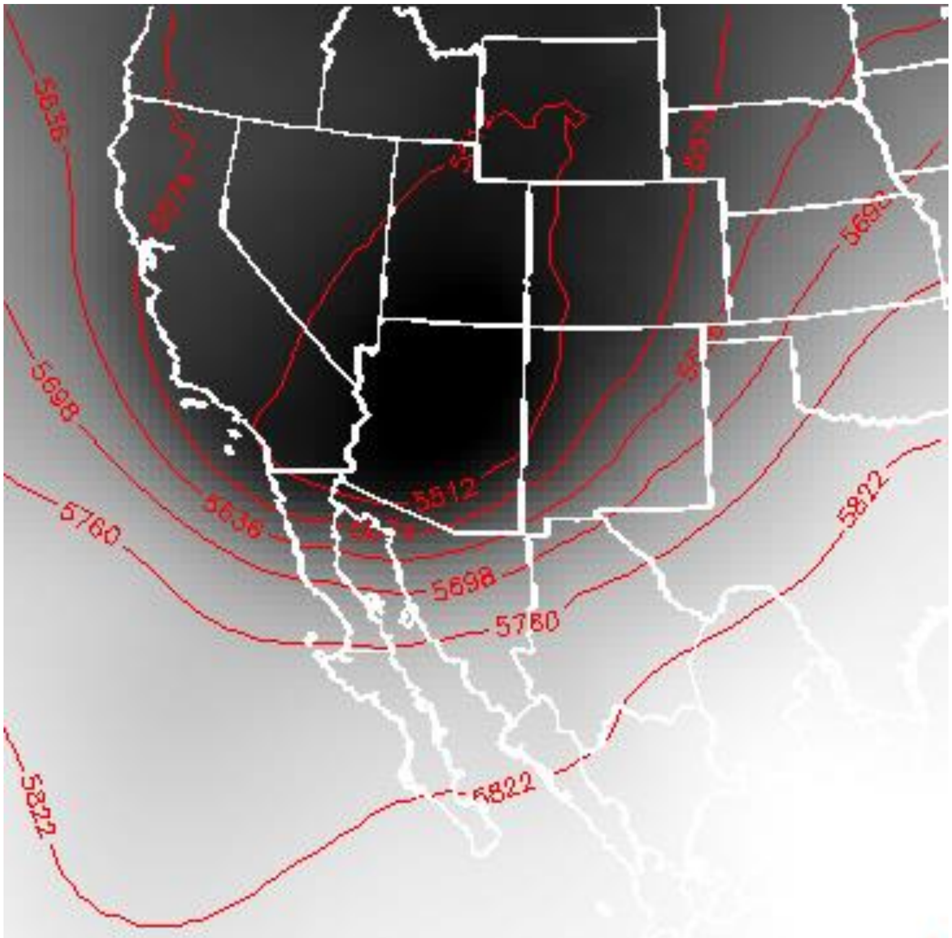

Figure 2.1.1. NARR geopotential height pattern (shaded background) for 14 April 2012 at 18 GMT overlaid with boundaries of the US and Mexican states as well as contour lines (shown in meters) of constant geopotential height in meters above ground level.

The satellite data, that were used to identify whether a dust storm exists, is from the Geostationary Operational Environmental Satellites (GOES). In particular, analysis of the longwave temperature difference image from the series of GOES satellites, determines if a dust event is recognized (or "seen") in the Northern Mexico/Southern New Mexico border region. The associated cyclone over the Utah/Nevada/Arizona border region is also recognized in the longwave temperature difference image as shown in Figure. 2.1.2.

Ackerman (1997) discusses the use of the brightness temperature differences between two sets of satellite infrared observations for dust detection. These differences are between 11 μm and 12 μm and 8 μm and 11 μm wavelength bands. The difference that was used in detecting the dust storms is BT11 – BT12 where BT is the "brightness temperature". This yields negative differences for dust aerosol and positive differences for other atmospheric features such as clouds which create a very distinct signature for the dust plumes. Additionally, because this technique is applied to the observations from the GOES satellites, very good temporal resolution (15min to 1hr) exists over a complete 24hr period. This is as opposed to the polar orbiting satellites where only a few observations per day are obtained and those may not be at opportune times.

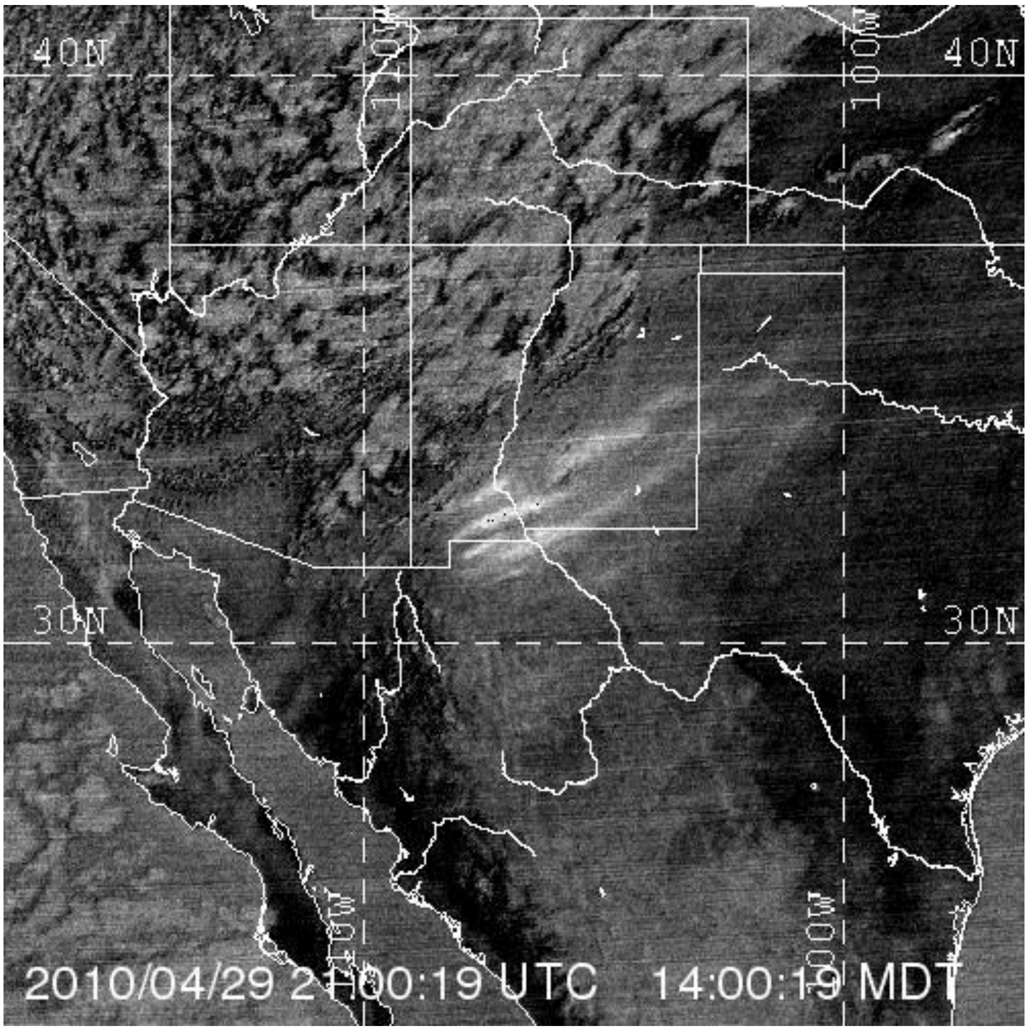

Figure. 2.1.2. Longwave temperature difference image for a dust event on 29 April 2010 at 21 GMT. This image is created by differencing the 11 micron and 12 micron image bands from a GOES satellite. The gray scale goes from white to black where white (dust plumes) values are negative and black values are positive. This allows for a very clear definition of the dust plume as it is seen in the multiple plumes aligned in a northeasterly direction in Southern New Mexico and Northern Mexico.

For recent times, this dataset is only available from the GOES sounder as opposed to the GOES imager and as such yields an approximate resolution of 10km (the imager was ~4km). The GOES sounder has poorer spatial resolution than does the imager because of major sensor differences. The archive of dust storm events was created using NMSU resources (the satellite ground stations within CARSAME) as well as those from the U.S. Regional and Mesoscale Meteorology Branch (RAMMB), which is hosted by the Cooperative Institute for Research in the Atmosphere, online at http://rammb.cira.colostate.edu/ramsdis/online/sounder.asp.

Figure 2.1.3 shows the locations of the dust plume sources for the complete archive of dust events from 2002-2014 overlaid on a map of major ecoregions in the Southwestern US/Northern Mexico border region. To make this study manageable, only dust events that occurred during January, February, March, April, and May for the years 2011-2014, and that were located along the New Mexico/Mexico border region (29-36 degrees north latitude, 104-112 degrees west longitude) (see Figure 2.2), were considered. This is shown in Figure 2.1.4 where the locations of this smaller plume source location dataset are overlaid on a map of the major ecoregions in the Southwestern US/Northern Mexico region along with a “box” that shows the locations of the actual dust events used in this study.

This reduced dataset resulted in a list of dust days that consisted of approximately 15 dust events per year (see Table 1 for list of dates). For the non-dust days, days for which there were no dust events in the whole of the Southwest US and Northern Mexico region were used. In addition, the day before and the day after the dust days were excluded. This resulted in a list of non-dust days that consisted of approximately 70 non-dust days per year. The list of dust days and non-dust days was used to select the NARR 500mb geopotential maps at 18 GMT that were used in this analysis. The reason for using the 18GMT NARR data was because this is the approximate time for dust storm initiation as is shown in Figure 2.1.5 that is a histogram of dust event start times for the dust events considered in this study. These start times were obtained from inspection of a time series of GOES longwave temperature difference images; some of which are only available once per hour in which case the start time is only to the closest hour.

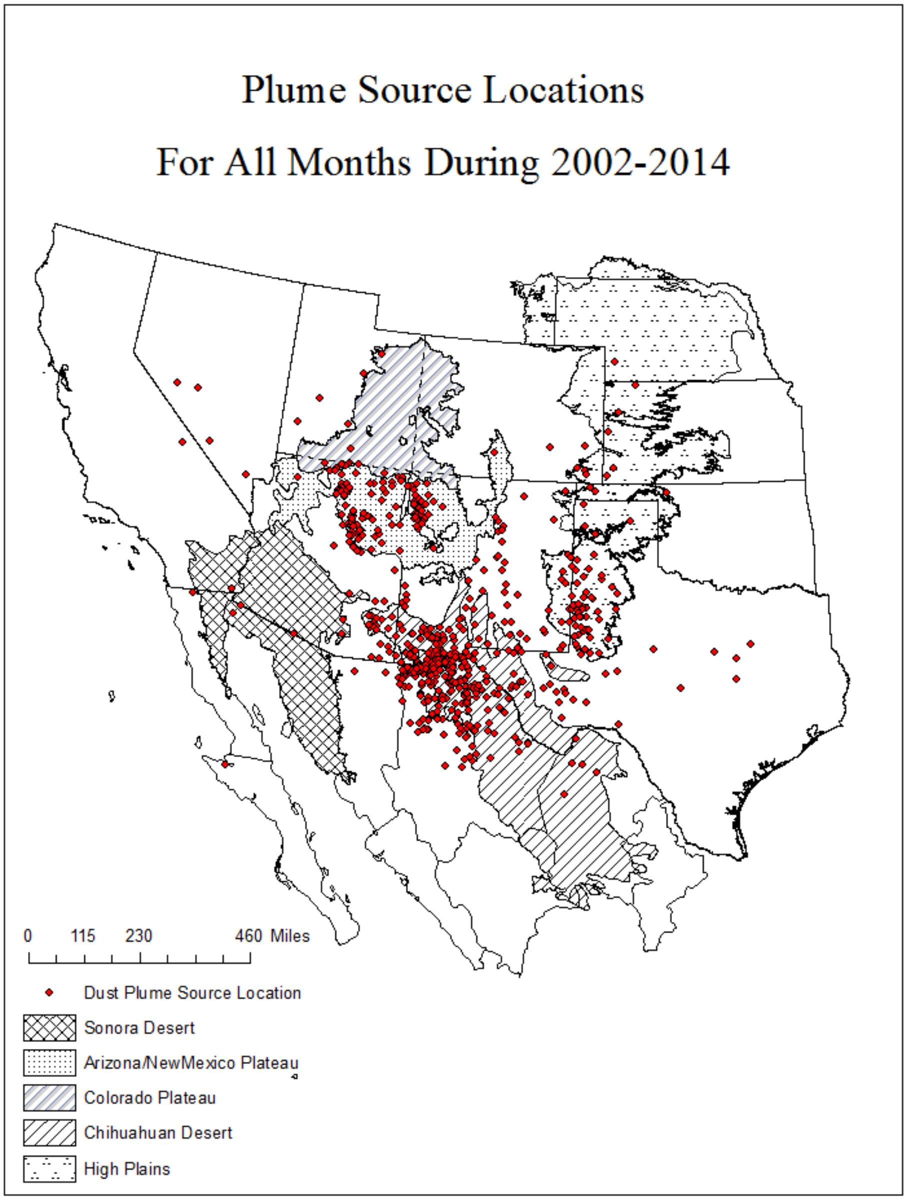

Figure 2.1.3 Plume source locations for all months during the period 2002-2014 overlaid on a map that shows the major ecoregions in the Southwestern US/Northern Mexico region (sources of shape files used to create the desert locations: Nolan, ca. 2003; Qi, 2010; Data Basin, 2016).

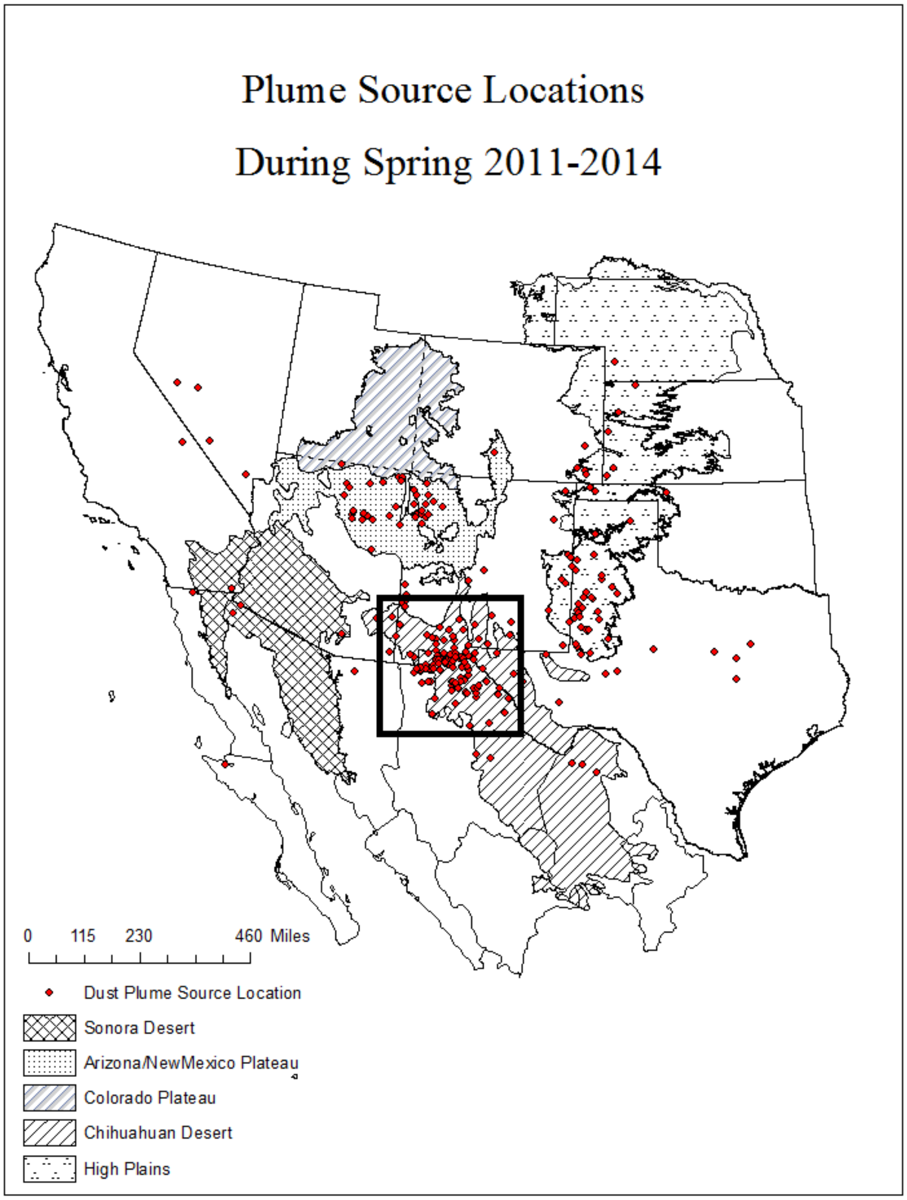

Figure 2.1.4 Plume source locations during the Spring of 2011-2014 overlaid on a map that shows the major ecoregions in the Southwestern US/Northern Mexico region along with a "box" that shows the locations of the dust events used in this study(sources of shape files used to create the desert locations: Nolan, ca. 2003; Qi, 2010; Data Basin, 2016).

Table 1. Dust day dates by year. This table lists the actual dates (mm/dd) for which there were dust events that were used in this study.

2011	**2012**	**2013**	**2014**
02/08	02/28	01/29	03/12
02/27	03/02	02/09	03/26
03/07	03/06	02/20	03/27
03/22	03/07	02/24	04/02
04/03	03/17	03/04	04/23
04/09	04/01	03/17	04/27
04/14	04/02	03/23	05/05
04/18	04/14	04/08	05/06
04/24	04/19	04/09	05/07
04/26	04/26	04/14	05/11
05/01	04/27	04/15	
05/19	05/02	04/16	
05/20	05/18	04/17	
05/28	05/19	04/25	
05/29	05/22	04/30	
	05/23	05/20	
	05/24		
	05/25		
	05/26		

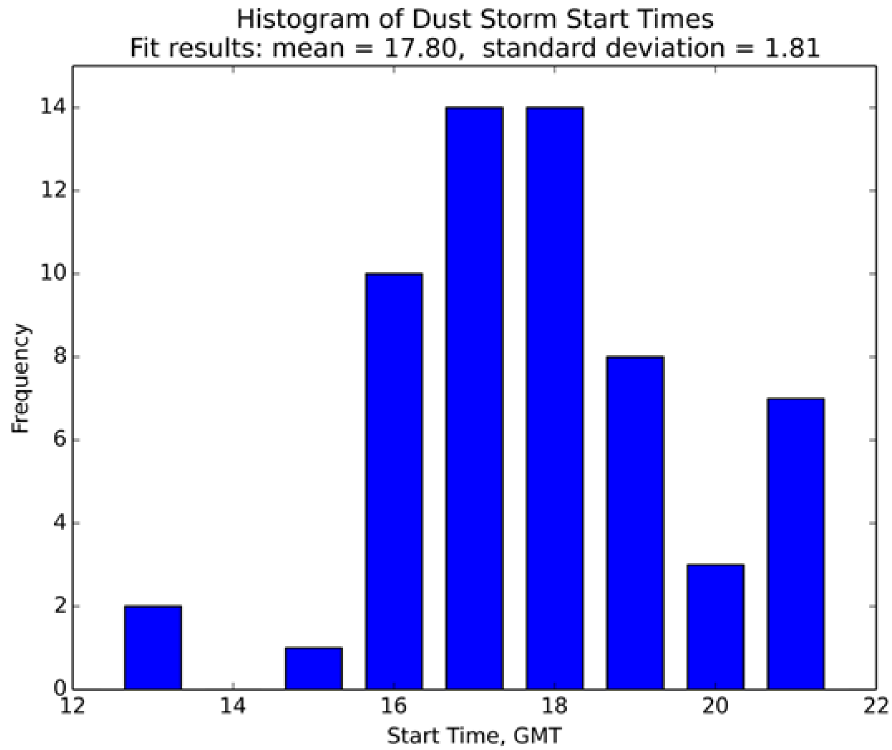

Figure. 2.1.5. Distribution of mean dust event start times. This histogram shows the distribution of dust event start times as determined from inspection of the sequence of dust event images with time for the years 2011, 2012, 2013, and 2014.

2.2 Methods

In order to answer the research question, a way to compare dust day patterns to a key dust day pattern for the 500mb geopotential height must be found. An accepted method in image processing to perform such a comparison is where two images are cross-correlated with one another (R. Lewis, 1990). The cross-correlation that is used here is basically the same as the Pearson product-moment correlation (Yarnal, 1993) with which most readers are familiar and is used to establish similarity between pressure pattern pairs. Yarnal (1993) used cross-correlation to determine prevalent synoptic climatology patterns of geopotential height. He then used those synoptic patterns to determine the conditions that exist during extreme environmental conditions, such as heavy rain fall and severe air pollution events. Through observational and anecdotal evidence, most likely the “Albuquerque low”, or, a somewhat similar pressure pattern, is responsible for dust events in our region. The equation that was implemented for analysis is given by equation (1) (Thoma, 2013).

$$ZNCC(Img_1, Img_2, u_1, v_1\ u_2, v_2, n) = \frac{\frac{1}{(2n+1)^2}\sum_{i=-n}^{n}\sum_{j=-n}^{n}\prod_{t-1}^{2}\left(Img_t(u_t+i, v_t+j) - \overline{Img}(u_t, v_t, n)\right)}{\sigma_1(u_1, v_1, n)\sigma_2(u_2, v_2, n)}$$

Equation (1)

Where:

ZNCC is the resulting cross − corelation between the image pairs
Img_1, Img_2 are the image arrays
σ_1 and σ_1 are the standard deviations of the gray levels in images 1 and 2,
$\overline{\text{Img}}$ is the average gray value and u and v are the u,v pixel location,

the images are square images of size $(2n+1) \cdot (2n+1)$, and (u_1, v_1) and (u_2, v_2) are the centers of the respective images

To facilitate the analysis, layer stacking of the dust day and non-dust day pressure patterns was used to create two single multi-band files for each year which were easier to subset and to then determine the descriptive statistics for the pressure patterns. For this, the software ENVI™ 4.8 was used. The layer stacking tool in ENVI™ 4.8 allows for multiple layers/images/bands of data arrays to be combined into a single multiple layer file where each layer has common geo-referencing and pixel size. For example, after layer stacking, the original NARR was subsetted from 349 samples (columns) and 277 lines (rows) to a 91 column by 91 row image to accommodate the Python code (implementing equation (1)) that was used to perform the cross-correlation between image pairs (Thoma, 2013). A listing of the code is given in Appendix C. The key pattern to which all of the individual daily patterns were compared was the yearly mean dust day pressure pattern. The mean non-dust day pressure pattern was also determined so that it could be used to compare the dust day and non-dust day pressure patterns in a qualitative way. These sets of results are shown in Figure 2.2.1 that displays the mean 500mb geopotential height patterns for dust days and non-dust days for each of the years studied: 2011, 2012, 2013, and 2014. It is observed that there is a trough over the Southwestern United States in the dust day mean for each year and that there is no such feature in the non-dust day mean patterns. The reason that the mean dust day pattern shows a trough as opposed to a very distinct low pressure feature is that each individual pattern that was used to create the mean had the center of the low in a slightly different location due to timing differences as well as whether the storm track was more northerly or more southerly. The effect of this is to smear the mean feature into a trough pattern. Additional differences between dust day and the non-dust day means are seen in the spacing and orientation of the contours of geopotential height as see in Figure 2.2.1. The dust day contours are oriented in a north/south east/west direction whereas the non-dust day orientation is rotated about 45 degrees to the east so that the contours are oriented in a north/easterly direction. Further, the contour spacing for dust day means are closer to one another than the contours in the non-dust day mean. In other words, the study area on dust days is to the east of the trough axis and during non-dust days, the study area is to the east of a building ridge. For the dust day processing, cross-correlation between each daily dust day pattern and the dust day yearly mean was performed. For the non-dust day processing, cross-correlations between each daily non-dust day pattern and the dust day yearly mean was performed.

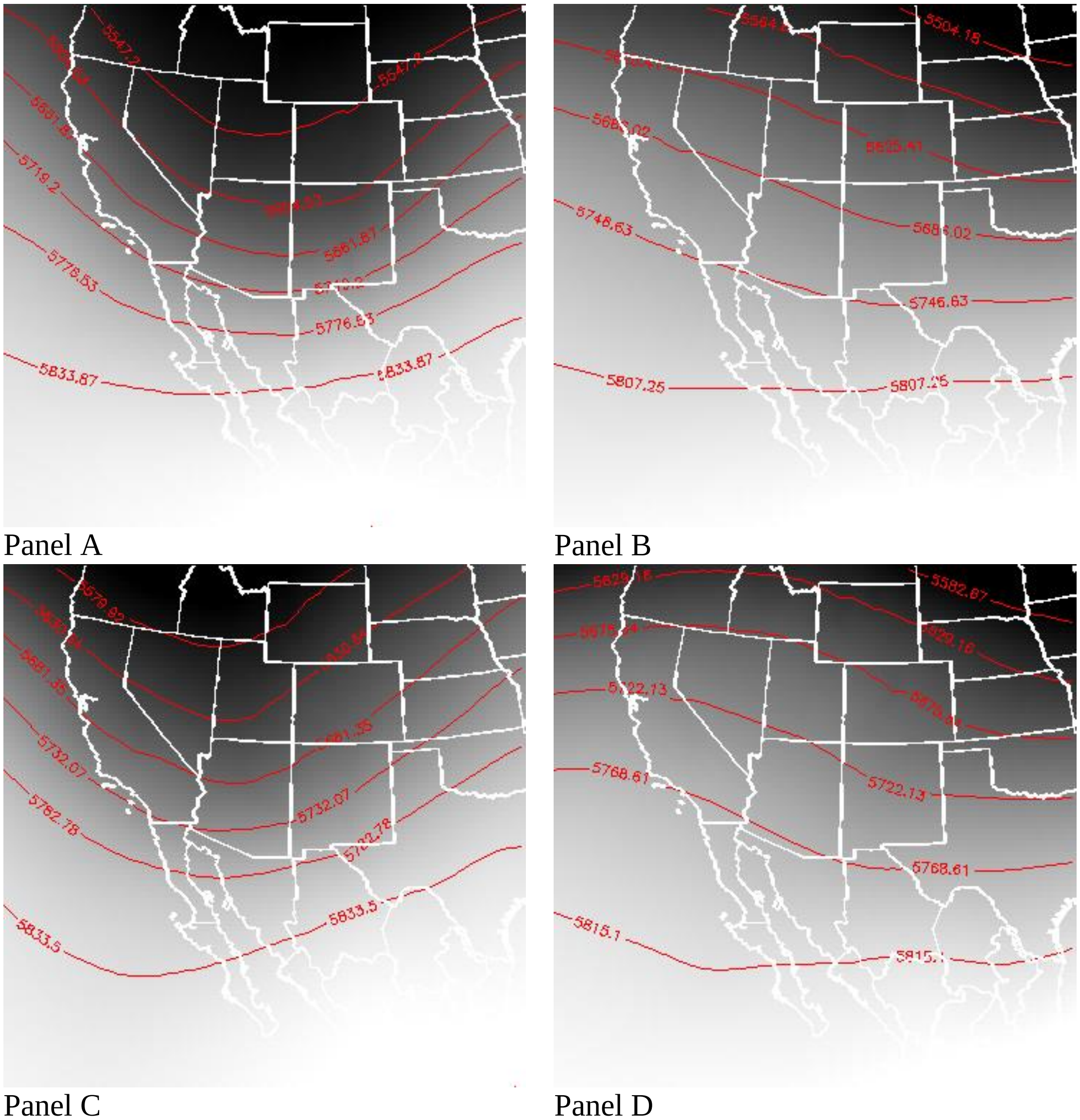

Figure 2.2.1. Mean 500mb geopotential height patterns (shaded background) from (A) 2011 dust day, (B) 2011 non-dust day, (C) 2012 dust day, (D) 2012 non-dust day. These mean 500mb geopotential height patterns at 18 GMT show the trough in the dust day mean and the lack of a similar feature in the non-dust day mean.

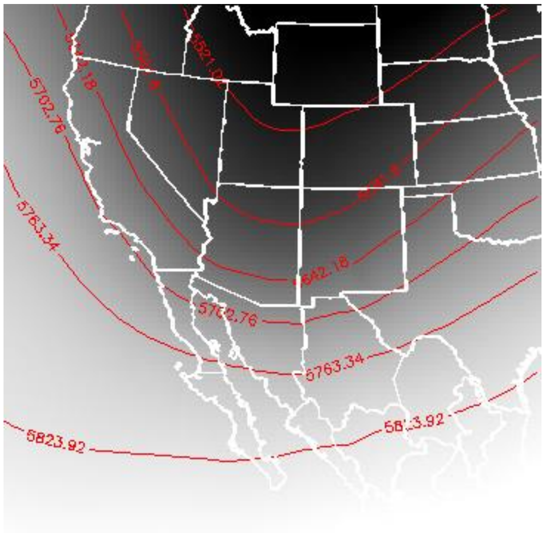

Panel E

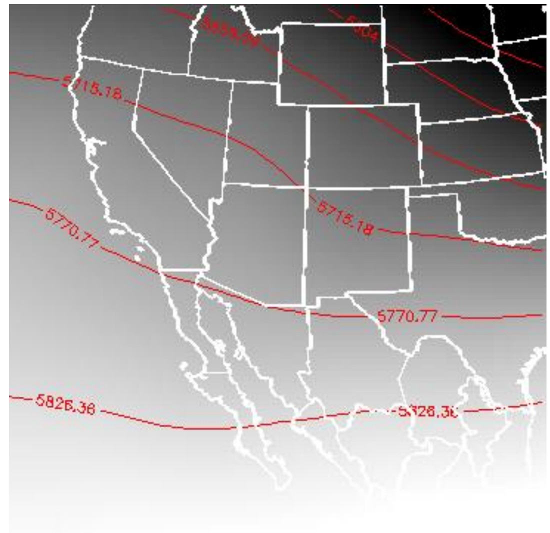

Panel F

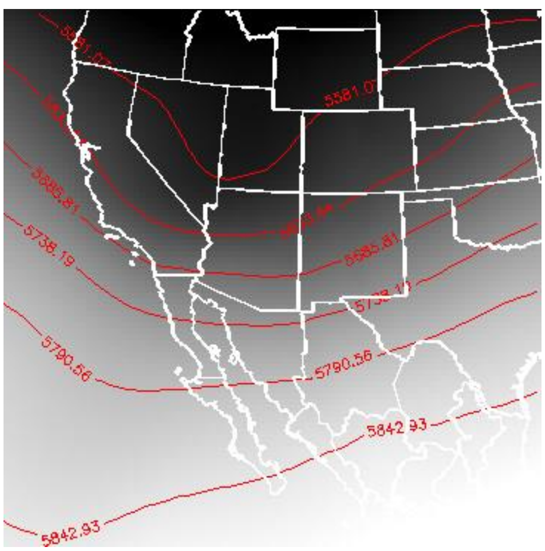

Panel G

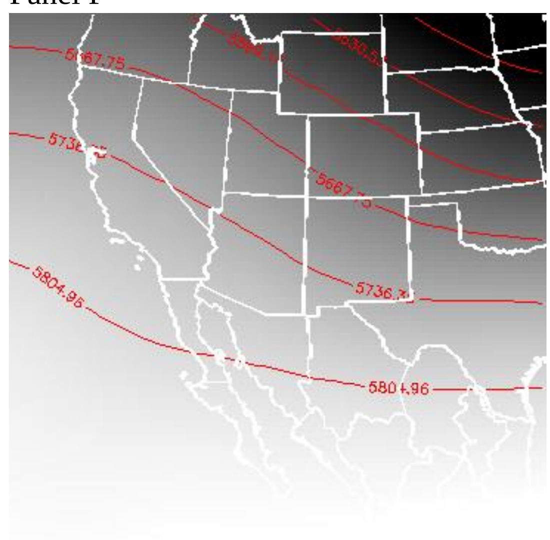

Panel H

Figure 2.2.1 (continued). Mean 500mb geopotential height patterns (shaded background) from (E) 2013 dust day, (F) 2013 Non-dust day, (G) 2014 dust day, (H) 2014 non-dust day. These mean 500mb geopotential height patterns at 18 GMT show the trough in the dust day mean and the lack of a similar feature in the non-dust day mean.

3.0 RESULTS AND DISCUSSION

A statistical analysis is necessary to determine the validity of the results and to complete the study (additional information on the statistical methods used in this study is given in Appendix D). Two distributions of cross-correlation results for each year need to be compared to determine if the two distributions are different and, hence, there is a difference in dust day and non-dust day patterns of the 500mb geopotential heights. Statistical methods are used to make this comparison. Most, if not all, statistical tests are based on certain assumptions which, if not met, yield invalid results. The first inclination was to use a parametric test as the data lends itself to that type of analysis; however, the usual parametric test to compare two distributions (Student's T-test) requires that the two distributions being compared be samples of normal distributions. After the fact, as explained in Appendix D, the SAS procedure UNIVARIATE was used to assess whether the distributions were samples of a normal distribution. In Figure 3.1, box plots from the SAS procedure UNIVARIATE showing the distributions of the correlation results for each of the four years are shown. Across all years, correlations were higher for dust days than for non-dust days. Additionally, the dust day distributions show less variance as well as having medians that are closer to their means also for dust days only during one year , 2011 was there an outlier correlation. For the non-dust day distributions the range of the data is larger than for the dust day and the variance for each non-dust day is also larger than that observed for the dust day distributions. For two years, 2011 and 2013 there are several outlier correlations. The statistical results from this procedure are given as the Shapiro-Wilk test statistic. These results are shown in Table 2 where it is seen that some of the distributions are not from normal populations ($P \geq 0.05$). Therefore, a non-parametric test is indicated.

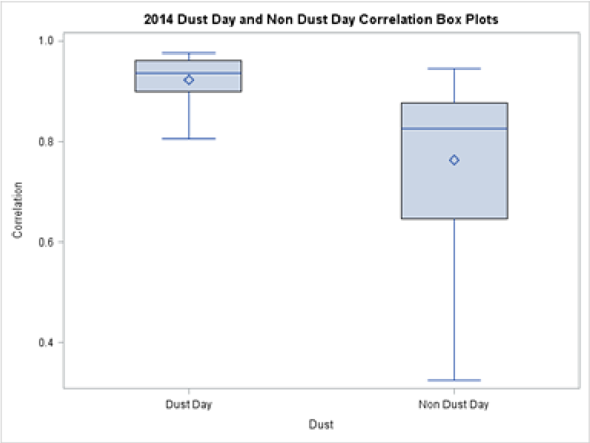

Panel A

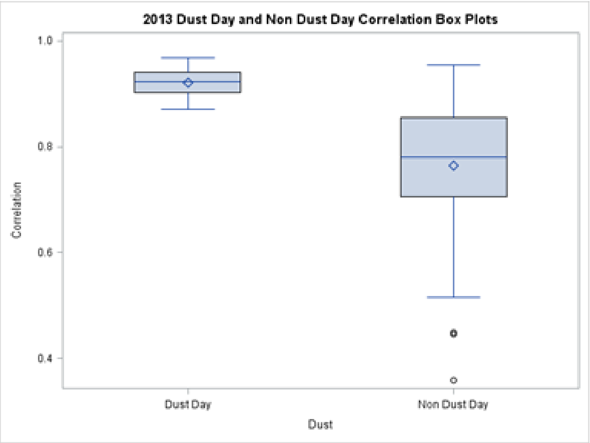

Panel B

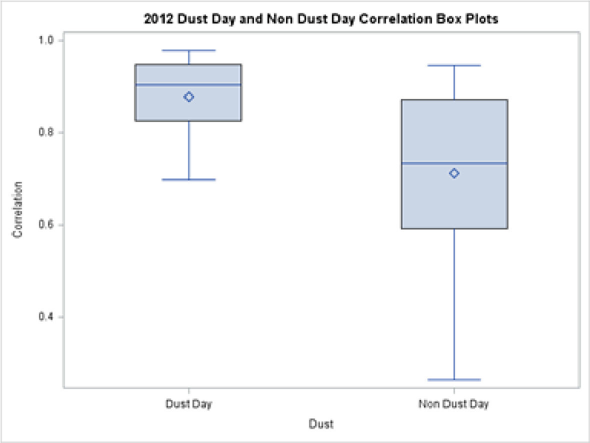

Panel C

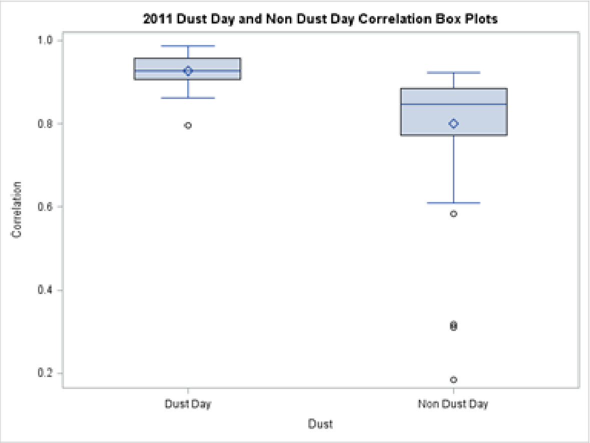

Panel D

Figure 3.1. Box plots from SAS procedure UNIVARIATE showing the distributions of the correlation data for each of the four years: Panel A is 2014, Panel B is 2013, Panel C is 2012, and Panel D is 2011.

The non-parametric statistical test that was used is the Wilcoxon Rank Sum Test and is implemented in the SAS procedure NPAR1WAY. The results of this test are given by the Kruskal-Wallis test statistic that uses the chi-square distribution for reporting its values. These are given in Table 3, where it is seen that for three of the years, the P-value is less than 0.0001 and for the other year, it is less than 0.0002. This means that the null hypothesis that tests equality of medians at a very high level of significance can be rejected. Therefore, there is a difference between the dust day distributions and the non-dust day distributions, which means that there is a particular 500mb 18GMT pressure pattern present at the beginning of the dust events in this study and that there is no such feature present during non-dust days.

It is of interest to note the height differences between the mean dust day geopotential heights and the mean non-dust day geopotential heights for the four years. The heights of the central point of the 91 by 91 height arrays are given in Table 4. The difference in height between the dust day and non-dust day heights ranges from a low of 26 to a high of 107.

Table 2. The Shapiro-Wilk test was used to determine whether the data in each year for dust days or non-dust days follow a normal distribution. P-values greater than the critical value of $\alpha = 0.05$ provide evidence that the non-dust day data are all from a normal distribution whereas all dust days are not.

Year	**Event**	**P-Value**
2011	Dust	P = 0.055
	Non Dust	P < 0.0001
2012	Dust	P = 0.0803
	Non Dust	P = 0.0068
2013	Dust	P = 0.8421
	Non Dust	P = 0.0015
2014	Dust	P = 0.0956
	Non Dust	P = 0.0001

Table. 3. The Kruskal-Wallis Chi-Square Statistic for each year is used to determine if there is a difference between the median of the distributions for dust days and non-dust days. P-values less than the critical value of $\alpha = 0.05$ provide evidence that there is a significant difference between distributions.

Year	2011	2012	2013	2014
P-value	< 0.0001	< 0.0001	< 0.0001	< 0.0002

Table 4. Geopotential heights for the central point of the 91X91 means geopotential height arrays that were created from the individual dust day and non-dust day patterns.

Year	**Non-Dust Day (m)**	**Dust Day (m)**	**Height Difference (m)**
2011	5732	5683	49
2012	5759	5733	26
2013	5757	5650	107
2014	5759	5690	69

4.0 CONCLUSION, RECOMMENDATIONS AND LIMITATIONS

4.1 Summary

The results of the previous section (Section 3) showed that significant progress has been made in understanding dust storm dynamics from the data acquired in this study, based on viewing many satellite images, and that there are specific 500mb geopotential height patterns necessary for the development of dust events. In particular, a region of low pressure to the north and west of our study area is responsible for producing conditions necessary for the initiation of dust storms along the Mexico/New Mexico border.

4.2 Recommendations

These results may be used by weather forecasters to develop tools for making forecasts of major dust events more accurate as well as for creating a climatology of dust events in our region. Specifically, results from this study can be used in two different ways: (1) The whole NARR dataset can be searched for possible dust day patterns to determine, over the past 35-year period, possible dust days that may be verified from satellite data archives, and (2) an Operational Forecast Tool can be developed that can use, for example, the North American Mesoscale Forecast System (NAM) or Global Forecast System (GFS) forecasted 500mb geopotential heights to search for possible dust days in the forecast. The forecast tool would be used at forecast offices to provide a notice that the models show a match to the key used in this study. This would create an alert to check other parameters such as time of day, antecedent precipitation conditions, as well as other conditions as are listed in Pollard (1978) and Novlan (2015).

4.3 Limitations

Two limitations of this research have been identified. The first limitation lies with the constraints imposed by the GOES imagery that allows for the identification only of larger dust plumes because the GOES imager is 4km spatial resolution and the GOES sounder is 10km spatial resolution. It is primarily the GOES imagery that has been used to recognize the presence of a dust event. Therefore, dust events from convective activity or those that are due to more localized winds are missed. Therefore, smaller and short-lived dust events as well as those occurring beneath the cloud cover will not be recorded in this archive. Events may have also been missed because of inattention to existing conditions.

The second limitation is the method that we chose for verifying the existence of a particular dust day key 500mb pressure pattern. A different, and possibly better, method would be to create a key pattern that is used in a template matching algorithm. Under this scenario, the location and strength of where the key pattern correlates strongly in the dust day pattern would result in a table of low pressure feature locations and strength depending on how well it matches the key pattern. One will then look for spatial clusters of high correlation data to be identified with dust events from a particular localized region.

Future work along these same lines would use a “feature matching” or “template matching” algorithm that would use a “low pressure feature” to search all of the 500mb geopotential height images for possible low pressure locations. These results would then be filtered and used, possibly, to define a relationship between the location of the low and the dust source region for all events in our inventory. And, of course, the requirement for determining source region characteristics prior to and during dust storm initiation is a critical part of understanding the total process; knowledge of the dust source location will facilitate that understanding.

To further enable an accurate forecast, besides the presence of the low pressure feature, it is necessary to consider other factors such as prior precipitation, vegetation cover, and disturbance level of the land surface at the site of the dust storm sources. Still other factors, will need to consider mesoscale dynamics.

APPENDIX A

COARSE LOCATION OF DUST STORM PLUMES

The contents of this appendix are from a standard operating procedure (SOP) that was developed for the New Mexico Environment Department (NMED) as documentation of the process that was used to locate dust storm plumes using coarse resolution satellite data along with semi quantitative tools.

STANDARD OPERATING PROCEDURE

FOR

NMSU Dust Source Location

SOP # AQXXX

NMSU
Center for Applied Remote Sensing in Agriculture, Meteorology and Environment
College of Agricultural, Consumer and Environmental Sciences
MSC 3BE, PO Box 30003
Las Cruces, NM 88003

Table of Contents

1 General Information

1.1 Principles and Applicability

This procedure describes the procedures used in the NMSU Dust Source Locaton. As this is not an instrument, no operation or service manual exists. This standard operating procedure was based on many hours of testing and operation in the laboratory and confirmed in independent analysis.

1.2 Summary of Method

The NMSU Dust Source Location technique was devised to allow someone who is not a remote sensing "expert" to identify dust storm plumes as seen in satellite imagery and to then determine the latitude and longitude for the sources of those plumes. Figure 1 shows an example of the satellite imagery that is used for these determinations. In actuality, instead of one image, several such images from a time sequence are observed by the technician to facilitate both the identification of the existence of a dust plume as well as from where it appears to originate.

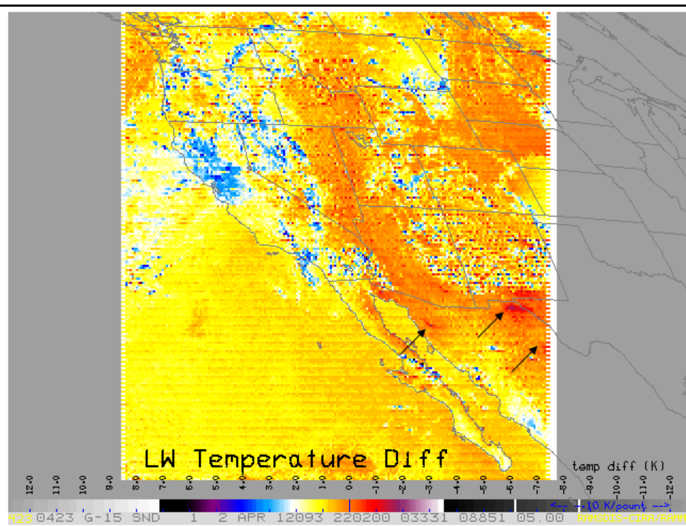

Figure 1. Figure 1 shows an example of the satellite imagery that is used to determine the locations of dust sources. The black arrows point towards three different dust plumes. This particular event occurred on 01/02 April 2012.

Table 1-1 provides the specifications for the Dust Source Location Protocol (At this time, there are no specifications.).

Parameter	Value

1.3 Definitions

This procedure uses the description for the Dust Source Location Protocol as provided under Section 1.2 above.

1.4 Health and Safety Warnings

There are no known health or safety issues associated with use of the Dust Source Location Protocol.

1.5 Cautions

There are no known cautions.

1.6 Interferences

There are no known interferences.

1.7 Personnel Qualifications

The Research Data Assistant is responsible for carrying out this standard operating procedure and for the completion and submission of all documents. Prior education/work experience in remote sensing data analyses/review is preferred.

The Laboratory Supervisor is responsible for overseeing the work, identifying and correcting deficiencies, and coordinating records transfer with the laboratory.

The Scientist-in-Charge is responsible for ensuring appropriate data download, reviewing data completeness, performing Level I and Level II review, initiating potential data processing troubleshooting investigations resulting from data review and other post processing data analysis activities.

2 Installation/Collection Procedures

2.1 Apparatus and Materials

2.1.1 Descriptions of Apparatus/Material

Computer for analysis with the software package ENVI installed as well as image viewing software (IrfanView) and software to record observational comments and data (EXCEL)

2.1.2 Reagents and Gases

N/A

2.1.3 Initial Startup

Dust Data Compilation from prior analysis/effort is required. This includes the date of the dust event and all collateral data such as wind records, dust forecasts, and satellite data from several sources.

2.2 Detailed Procedures

Example of identifying a dust source location and recording that information.

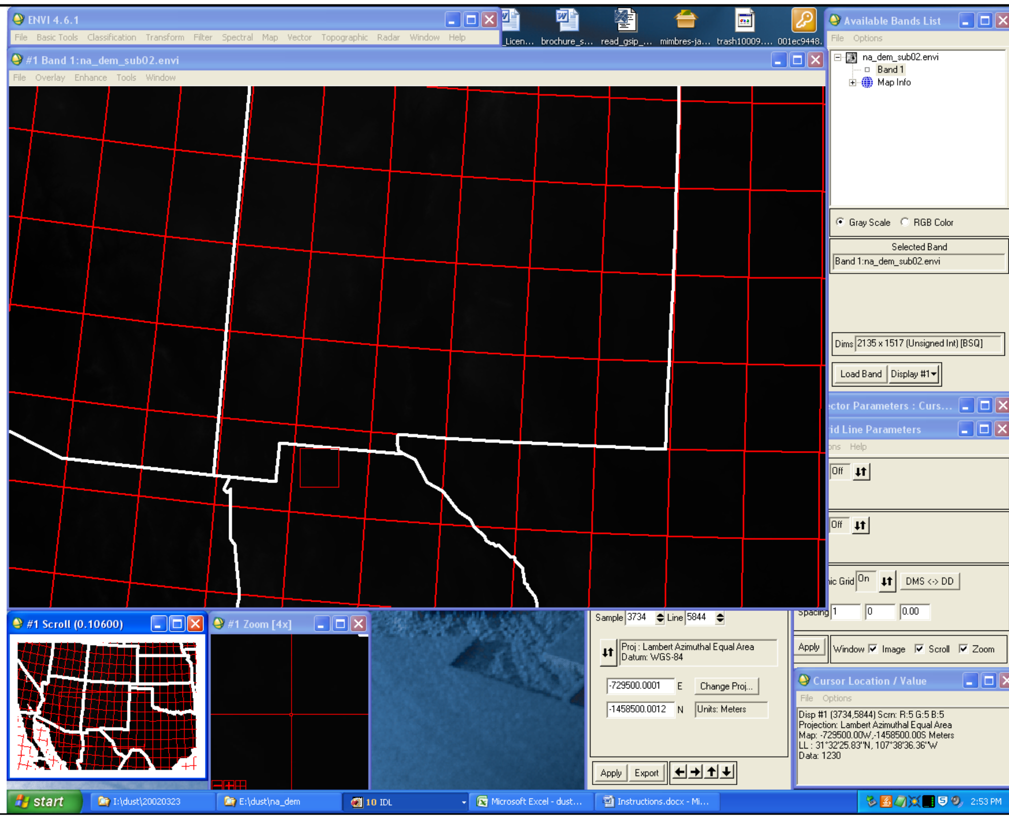

Figure 2. Example of how the computer screen will appear after completing the following steps.

Open ENVI 4.6.1. Select “File” → “Open Image File” and open file called “na_dem_sub02.envi” (E:\dust\na_dem).

The “Available Bands List” window will pop up, where you will click “Load Band” and three windows called “Band,” “Scroll,” and “Zoom” will also pop up. Enlarge “Band” window to your desired size.

Within the “Band” window, select in the drop-down menu “Overlay” → “Vectors.” Within the “Vector Parameters” window that pops up, select “File” → “Restore Layers from Template.” The only file that will pop up will be “states.vec,” open it.

In the “Vector Parameters” window, change the “Window” setting to “Off” and hit “Apply.”

In the “Band” window, select in the drop-down menu “Overlay” → “Grid Lines.” In the “Grid Line Parameters” window, select “File” → “Restore Setup.” A window with the option “grid.grd” will pop up, open the file. Hit “Apply” in the “Grid Line Parameters” window.

In the “Band” window, select “Tools” → “Cursor Location/Value” and “Tools” → “Pixel Locator.”

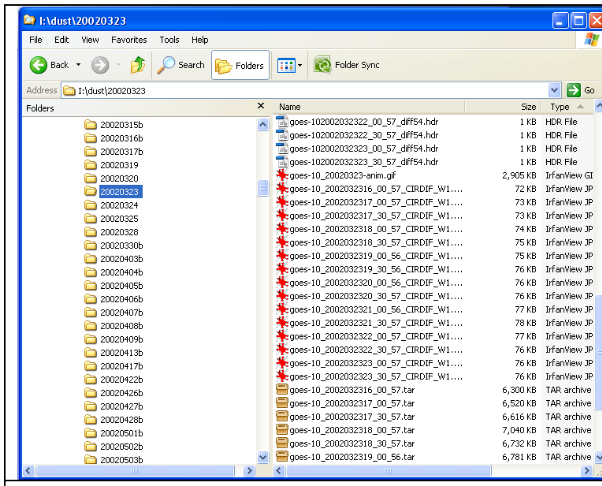

Figure 3. Windows Explorer view of the “dust archive”.

Bring up dust archive (I:\dust) and select directory for a specific day, such as “20020323.” Within each day’s directory, look for “goes” files (gw… or ge… in later dates) in either .gif or .jpg format. Most days with .gif files will have an accompanying animated .gif file. If there is no animated file or if the animation moves too quickly to discern where the dust originates, select an individual goes file and use the scrolling bar on your mouse to navigate between each time-stamped image.

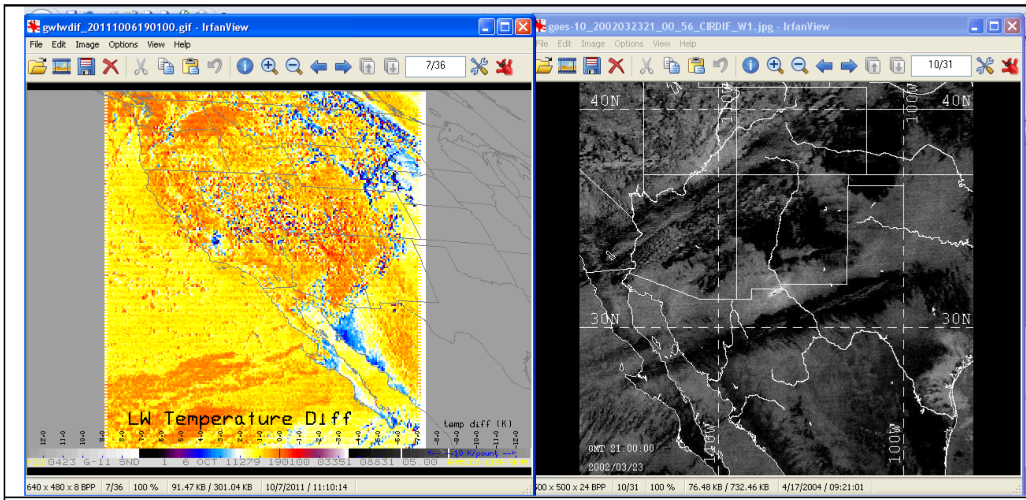

Figure 4. Two examples of how dust plumes appear in two different renditions of satellite imagery. The left panel is a false color representation of the GOES satellite brightness temperature difference between the two far-infrared channels. The right panel is a gray scale representation of the GOES satellite brightness temperature difference between the two far-infrared channels. Both of these examples are low spatial resolution examples that are being used for “coarse” location of the dust plumes. Follow-on work will utilize higher spatial resolution imagery for better specification of the dust plume source location.

In the black and white images (Figure 4, right panel), look for a concentrated area of white, which will likely be travelling in an eastward direction. In the above image, the dust storm is located just south of the New Mexico/Mexico border. In the color Infranview images (Figure 4, left panel), look for a concentrated area of red. In the above image, the dust storm is located in the northeastern corner of Arizona. We are looking for where the dust storm originates, not where it is the strongest, so look for where it appears in the earliest-time-stamped image, and it will probably have originated at the point farthest west. Sometimes you will be able to see a distinct needle-point shape in the dust cloud.

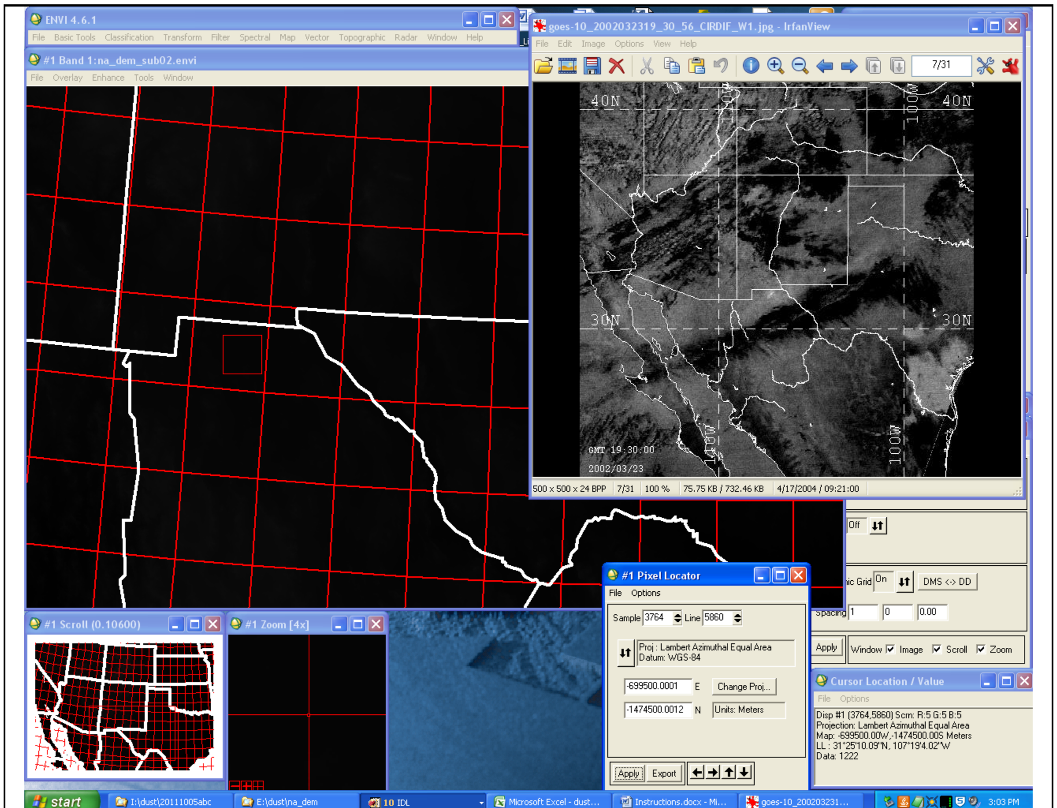

Figure 5. An example of how the computer screen will appear when attempting to determine the location of the dust plume (white form just below the NM/MX border). The small red box in the upper left portion of the image is the approximate location of the plume as identified by the operator. The resulting location information is displayed in other windows shown in the screen capture.

Once you have found the dust storm, use the “Scroll” window (see Figure 5) to select the larger area where the dust plume is located. Then, as accurately as possible, find the origin of the dust storm in the “Band” window. Use the gridlines to your advantage by estimating in the goes animation where the point is located, such as “¼ the height of the state of New Mexico, and about halfway across,” then applying it to the grid lines.

Click the location of the dust storm in the “Band” window, which will pull up the location in the “Zoom” window. Click the appropriate area in the “Zoom” window, and then in the “Pixel Locator” window, hit “Apply.” Now, you should be able to copy and paste the location of the dust storm from the “Cursor Location/Value” window into your Excel spreadsheet along with the day the goes images were taken. Example: 2002.03.23 → LL : 31°24'15.29"N, 107°24'1.48"W

2.2.7 Troubleshooting

N/A.

2.2.7 Documentation

This SOP is the documentation

2.3 Sample Laboratory Analysis and Calculation

N/A

2.3 Instrument or Method Calibration

N/A

3 Quality Control and Quality Assurance

The QC/QA procedures consist of performing the above analysis by different analysts and comparing the results. It is unknown, at this time, to what degree it can be expected for the results to “overlap” and how closely they will overlap.

3.1 Routine Service Checks

3.1.1 General Information

3.1.2 Frequency of Quality Control Checks

3.2 Detailed Maintenance Procedures

3.5 Checklist

N/A

4 Forms

None

5 References

none

6 Appendix

APPENDIX B

GEOPOTENTIAL HEIGHTS

The National Weather Service defines geopotential height as:

"In meteorology, usually a reference to **Geopotential Height**; roughly the height above sea level of a pressure level. For example, if a station reports that the 500 mb height at its location is 5600 m, it means that the level of the atmosphere over that station at which the atmospheric pressure is 500 mb is 5600 meters above sea level. This is an estimated height based on temperature and pressure data" (http://w1.weather.gov/glossary/index.php?letter=h).

Because cold air is heavier than warm air, the geopotential energy occurs at a lower attitude above sea level than the warm air. This means that the geopotential height is lower in cold air regions and higher in warm air regions. (http://ww2010.atmos.uiuc.edu/(Gh)/guides/mtr/cyc/upa/trgh.rxml).

500mb Geopotential Height Example (Wallace and Hobbs (2006):

In order that we are able to calculate geopotential height, we must begin with the ideal gas law:

$$p = n_0 kT$$

where:

p is pressure (Pa)
n_0 is number of molecules per unit volume
k is Boltzmann's constant (1.3806488×10^{-23} J K^{-1})
T is temperature (K)

For the partial pressure of the water vapor in the atmosphere,

$$e = \rho_v \, R_v T$$

where:

e is partial pressure of water vapor
ρ_v is the density of water vapor
R_v is the gas constant for 1kg of water vapor (461.5 J K^{-1} kg^{-1})
T is temperature (K)

From these, we can now get the equation for virtual temperature which is necessary for the determination of geopotential height. This is given by:

$$T_v \equiv \frac{T}{1 - \frac{e}{p}(1 - \varepsilon)}$$

Where:

> T_V is virtual temperature
> e is partial pressure of water vapor
> T is temperature (K)
> p is pressure (Pa)
> ε is 0.622 – ratio of molecular weight of water to molecular weight of dry air

The virtual temperature is the temperature that dry air would have the same density of moist air at the same pressure – there is rarely much difference between the two, however. We will need this later to determine the actual geopotential height.

We now move on to the hydrostatic equation that describes the relationship between the vertical forces acting on a cross-sectional area of of column of air. It states that the change in pressure with height is equal to the air density times the gravitational constant:

$$\frac{\partial p}{\partial z} = -g\rho$$

From here, we move on to the geopotential, Φ, which is "defined as the work that must be done against the Earth's gravitational field to raise a mass of 1 kg from sea level to that point":

$d\Phi \equiv g dz$

From this, the geopotential at height z is:

$$\Phi(z) = \int_0^z g dz$$

And then, the definition of the geopotential height is:

$$Z \equiv \frac{\Phi(z)}{g_0} = \frac{1}{g_0}\int_0^z g\,dz$$

where:

g_0 is the globally averaged value of the acceleration due to gravity at the earth's surface –9.81 m s^{-2}

And the geopotential height is basically the same as geometric height because the acceleration of gravity varies little with altitude until one gets above about 100 km.

To determine the geopotential height for a particular pressure level, we must now consider the hypsometric equation:

$$Z_2 - Z_1 = \bar{H}\ln\left(\frac{p_1}{p_2}\right) = \frac{R_d\bar{T}_v}{g_0}\ln\left(\frac{p_1}{p_2}\right)$$

where:

$\bar{H}$ is the average "scale height" (~8 km)
$\bar{T}_v$ is the mean virtual temperature of the layer between the two levels
p_0 is surface pressure (hPa)
p_1 is pressure at some level (e.g., 500hPa) (hPa)
R_d is the gas constant for 1kg of dry air (287.0 J K^{-1} kg^{-1})

Then,

$$Z_{some\ level,hPa} - Z_{sea\ level} = \bar{H}ln\left(\frac{p_{sea\ level}}{p_{some\ level}}\right)$$

$$Z_{some\ level,hPa} - Z_{sea\ level} = \bar{H}ln\left(1 + \frac{p_{sea\ level} - p_{some\ level}}{p_{some\ level}}\right)$$

$$Z_{some\ level,hPa} - Z_{sea\ level} \approx \bar{H}\left(\frac{p_{sea\ level} - p_{some\ level}}{p_{some\ level}}\right)$$

and, because $Z_{sea\ level} = 0$, and with the scale height of 8000m,

we get:

$$Z_{some\ level,hPa} \approx 8(p_{sea\ level} - p_{some\ level})$$

So, if sea level pressure is 1013hPa and some level is 500 hPa, then we get 513*8=4104.

However, this does not take into account the atmospheric temperature; so, we must go back to the hypsometric equation:

$$Z_2 - Z_1 = \frac{287.0 * \bar{T}_v}{9.81} ln\left(\frac{p_1}{p_2}\right)$$

For the thickness between sea level and 500mb, we get

$$Z_{500\ hPa} - Z_{1013\ hPa} = \frac{287.0 * \bar{T}_v}{9.81} ln\left(\frac{1013}{500}\right)$$

$$Z_{500\ hPa} - Z_{1013\ hPa} = 29.26 * \bar{T}_v * 0.706$$

$$Z_{500\ hPa} - Z_{1013\ hPa} = 20.65 * \bar{T}_v$$

In the tropics, the virtual temperature is ~15°C and at the poles, it is ~-40°C; or, in Kelvin, 288K and 233K, respectively. ΔZ in tropics is ~5948m and at poles ~4812m. If we take the sea level altitude to be zero, then, these are our geopotential heights.

APPENDIX C

Python computer code used for Cross-correlation

```
#!/usr/bin/env python
# -*- coding: utf-8 -*-
import sys
from scipy.misc import imread
from scipy.linalg import norm
from scipy import sum, average
import matplotlib.pyplot as plt
from scipy import ndimage
from scipy import signal
import numpy as np
import os
import os.path
import sys
global ext
import glob
import csv
#from pylab import *
#
#I'll assume you have a part of both image of size (2n+1)×(2n+1).
#The pixel in the center has coordinates (u1,v1)
#for the part of the first image and (u2,v2) for the second
image.
#
#   20150607:  will modify to use binary arrays as inputs... so,
#   will need to open, for the NARR data, the ENVI files created
#   for the dust days and non-dust days
#
#   20150618:  am modifying to take the nam forecasted patterns
and
#   perform the zncc in a for loop configuration
#
def main():
# read images as 2D arrays
#
#   need to read in the forecasts for a particular date and cycle
#   and then process and output results to a text file and do the
#   scatter plots -- eventually, will want to plot the zncc
results, as well
#
    mydir= '/media/xtuser/Armenta/500dust_days/2011_20150622/'
    file_list = sorted
(glob.glob('/media/xtuser/Armenta/500dust_days/2011_20150622/500m
b_2014_dustday_91X91_????.dat' ))
    #print file_list[:]
    #print len(file_list)
    #sys.exit()
```

```
#
#   get basename
#
#day = os.path.basename(netCDF)
    for index in range(len(file_list)):
        day = os.path.basename(file_list[index])
        forecast_file = mydir + '/' + day
        #print forecast_file
        #print day


#  now, need to strip out the _ -- also, it would be good to lose
the path part of the name --that way
#  we can make it more general as we go from one machine to the
other
#
        year = day[6:10]
        print year
        month= day[25:27]
        doy = day[27:29]
        print month
        print doy
        #sys.exit()

        new_array1 =
np.fromfile('/media/xtuser/Armenta/500dust_days/2011_20150622/500
mb_2014_dustday_91X91_Stats_Mean.dat', dtype='float32', count=-1,
sep="")
        new_array2 = np.fromfile(forecast_file, dtype='float32',
count=-1, sep="")
    #new_array =
np.fromfile('/home/max/pythonpractice/save165.dat', dtype='d',
count=-1, sep="")
#    print 'new_array1.shape', new_array1.shape
        new_array1_2d = new_array1.reshape(91,91)
        new_array1_2d_flip = np.flipud(new_array1_2d)
        new_array2_2d = new_array2.reshape(91,91)
        new_array2_2d_flip = np.flipud(new_array2_2d)
#    print 'sub03 mean \n'
#    print new_array1_2d
        img1 = new_array1_2d
        img2 = new_array2_2d
#    compare
#    n_m, n_0 = compare_images(img1, img2)
#    print file1, '\n',file2
#    print "Manhattan norm:", n_m, "/ per pixel:", n_m/img1.size
#    print "Zero norm:", n_0, "/ per pixel:", n_0*1.0/img1.size
#    print  "zero-norm cc:",zncc(img1, img2, 199,199,199,199,
200)
        correlation = zncc(img1, img2, 44,44,44,44, 45)
```

```
        print  "zero-norm cc:",correlation
        correlation_str = str(correlation)
        print correlation_str
        plt.rc('axes', linewidth=2)
# Make a dummy plot
    #plot([0, 1], [0, 1])
        plt.plot([5000,6000], [5000,6000])
# Change size and font of tick labels
# Again, this doesn't work in interactive mode.
        fontsize = 14
        ax = plt.gca()
#        print ax
# Plot
#    print img1, img2
    #ax.scatter(img1, img2, s=1, c='black', marker=u'o')
        ax.scatter(img1, img2, s=1, c='black', marker=u'.')
        ax.set_xlim(5000, 6000)
        ax.set_ylim(5000, 6000)
        plt.grid(True)
        ax.set_title('Day of Dust Event:  ' + year + month + doy
+ '\n' + 'zero-norm cross-correlation = ' + correlation_str)
        plt.xlabel(r"mean", fontsize = 12)
        plt.ylabel(r"Observed", fontsize = 12)
#
#       need to add the zero-norm cc...
#

        plt.savefig(mydir + 'scatter' +  '_' + year + '_' +
month + '_' + doy + '.png', dpi=600)
        with open(mydir + 'zncc_' + year + '.csv', 'a') as ofile:
            writer = csv.writer(ofile, delimiter=',')
            writer.writerow([year, month, doy, correlation])
            ofile.close()
        plt.close("all")
#        plt.show()
#    xlabel('X Axis', fontsize=16, fontweight='bold')
#    ylabel('Y Axis', fontsize=16, fontweight='bold')
# Save figure
#
plt.savefig('/home/xtuser/dust_python/max_grib/dust_20130502.png'
, dpi=600)
#    print  "zero-norm cc:",zncc(img1, img2, 162,162,162,162,
163)
#    ndarray = signal.correlate2d(img1, img2)
#    print ndarray
#    print array.max(ndarray)
#    plt.imshow(ndarray)
#    plt.show()

def compare_images(img1, img2):
    # normalize to compensate for exposure difference
```

```
    img1 = normalize(img1)
    img2 = normalize(img2)
    # calculate the difference and its norms
    diff = img1 - img2  # elementwise for scipy arrays
    m_norm = sum(abs(diff))  # Manhattan norm
    z_norm = norm(diff.ravel(), 0)  # Zero norm
    return (m_norm, z_norm)

def to_grayscale(arr):
    "If arr is a color image (3D array), convert it to grayscale
(2D array)."
    if len(arr.shape) == 3:
        return average(arr, -1)  # average over the last axis
(color channels)
    else:
        return arr

def normalize(arr):
    rng = arr.max()-arr.min()
    amin = arr.min()
    return (arr-amin)*255/rng

def zncc(img1, img2, u1, v1, u2, v2, n):
    stdDeviation1 = ndimage.standard_deviation(img1)
    stdDeviation2 = ndimage.standard_deviation(img2)
    avg1 = ndimage.mean(img1)
    avg2 = ndimage.mean(img2)
#    print avg1,avg2
    s = 0
    for i in range(-n, n+1):
        for j in range(-n, n+1):
            s += (img1[u1+i][v1+j] - avg1)*(img2[u2+i][v2+j] -
avg2)
    return float(s)/((2*n+1)**2 * stdDeviation1 * stdDeviation2)

if __name__ == "__main__":
#    A  = [[1,2,3],[4,5,6],[7,8,9]]
#    B1 = [[1,2,3],[4,5,6],[7,8,9]]
#    B2 = [[1,2,3],[4,5,6],[7,8,7]]
#    print(zncc(img1, img2, 1,1,1,1, 1))
#    print(zncc(A, B2, 1,1,1,1, 1))
    main()
```

APPENDIX D

STATISTICAL ANALYSIS

In this appendix, the overall statistical analysis approach was used is discussed with more detail. In statistical analysis, there are two approaches to hypothesis testing that can be used. The first is parametric analysis that is used to make inferences about populations with normal distribution with ratio and interval types of data. The other type of analysis is non-parametric analysis that does not assume that the data are from a population with a normal distribution. This non-parametric analysis general uses ordinal or nominal scale datatype. In this research, based on initial thoughts the parametric Student's T-test (using procedure T-test form the SAS software (version 9.4)) was first applied to determine if the population means for dust day and non-dust day correlation results were the same. Investigation of the T-test results indicated that the distribution being tested may not have been from normal populations to confirm this thought, a procedure called UNIVARIATE in the SAS software was used as a test for normal distributions. The results from that test showed that the non-dust day distributions were from normal distribution; however, the dust day distributions were shown to be from non-normal populations. Therefore, it was necessary to investigate non-parametric statistical analysis. The advice from the statistical consultants stated that the Wilcoxon Rank Sum test was appropriate. This test was implemented in SAS software the procedure NPAR1WAY. The output from all three of these procedures are given in the remainder of this appendix.

D.1 TTEST:

The SAS code that was used to generate the following TTEST results:

```
proc import
	out = dust
	datafile = 'F:\SAS/2013_stats_dustday_nondustday_SAS'
	replace
	dbms = xlsx;
run;

proc print data = dust;
run;

proc ttest data = dust sides=2 alpha=0.05 h0=0;
	class dust;
	var correlation;
	Title "2013 Dust Day and Non Dust Day Ttest";
run;

proc sgplot data = dust;
	vbox correlation / category = dust;
	Title "2013 Dust Day and Non Dust Day Correlation Box Plots";
run;
```

In Table D.1.1, SAS t-test results for the Null Hypothesis of cross-correlation results: $\mu_{dust} = \mu_{non\text{-}dust}$ are shown. The results indicate, without regard to the Test of Equality of Variances, that the Null Hypothesis is rejected at Pr > |t| for t less than or equal to .005. However, if we take into account the Test of Equality of Variances, in all four years, then we should consider unequal variances in which case the t-test results reject equality of means at a probability less than .0001. The complete output for the SAS procedure are given in this Appendix.

Table D.1.1. SAS t-test results for the Null Hypothesis of cross-correlation results: $\mu_{dust} = \mu_{non\text{-}dust}$.

Year	**Method**	**Variances**	**DF**	**t Value**	**Pr > |t|**
2011	Pooled	Equal	92	3.55	0.0006
	Satterthwaite	Unequal	62.078	6.41	<.0001
2012	Pooled	Equal	81	4.09	0.0001
	Satterthwaite	Unequal	61.176	5.74	<.0001
2013	Pooled	Equal	86	4.82	<.0001
	Satterthwaite	Unequal	85.834	9.29	<.0001
2014	Pooled	Equal	85	3.12	0.0025
	Satterthwaite	Unequal	36.159	6.42	<.0001

SAS TTEST Results

2011 Dust Day and Non Dust Day Ttest

The TTEST Procedure

Variable: Correlation (Correlation)

Dust	N	Mean	Std Dev	Std Err	Minimum	Maximum
Dust Day	15	0.9265	0.0483	0.0125	0.7966	0.9867
Non Dust Day	79	0.8004	0.1353	0.0152	0.1838	0.9231
Diff (1-2)		0.1261	0.1260	0.0355		

Dust	Method	Mean	95% CL Mean		Std Dev	95% CL Std Dev	
Dust Day		0.9265	0.8998	0.9532	0.0483	0.0354	0.0762
Non Dust Day		0.8004	0.7701	0.8307	0.1353	0.1170	0.1604
Diff (1-2)	**Pooled**	0.1261	0.0556	0.1966	0.1260	0.1101	0.1472
Diff (1-2)	**Satterthwaite**	0.1261	0.0867	0.1654			

Method	Variances	DF	t Value	Pr > |t|
Pooled	Equal	92	3.55	0.0006
Satterthwaite	Unequal	62.078	6.41	<.0001

Equality of Variances

Method	Num DF	Den DF	F Value	Pr > F
Folded F	78	14	7.85	0.0001

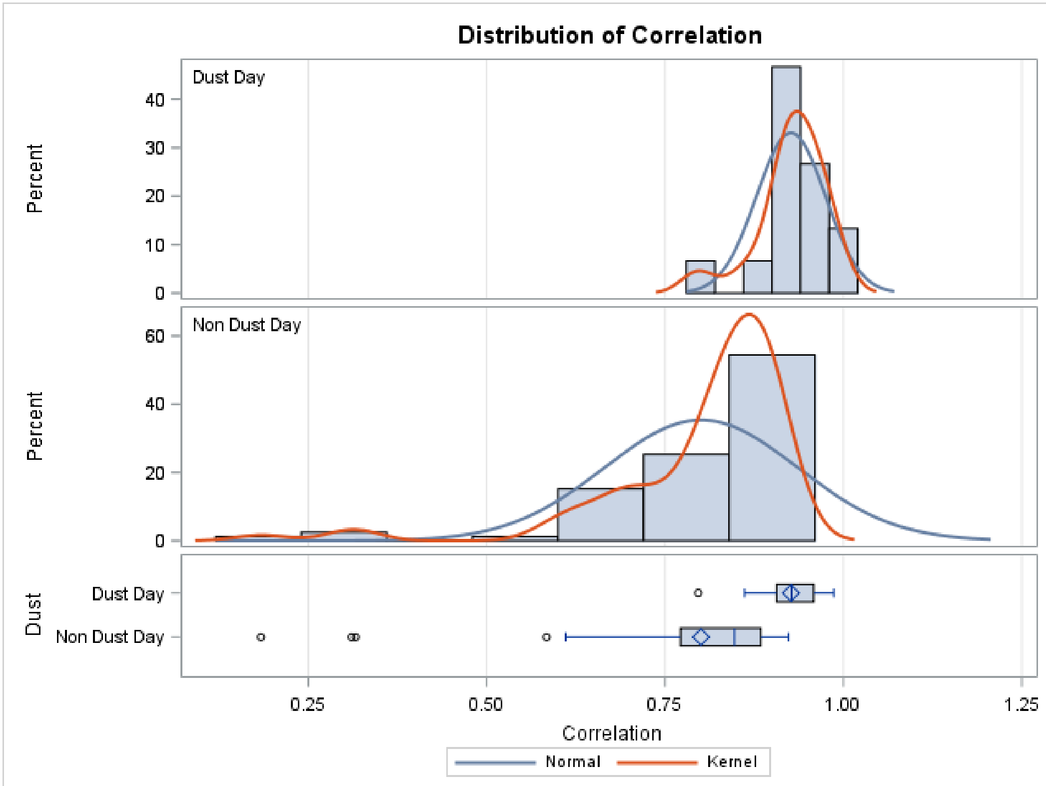

Distribution of Correlation
Dust Day
Non Dust Day
Percent
Dust
Dust Day
Non Dust Day
0.25
0.50
0.75
1.00
1.25
Correlation
Normal
Kernel

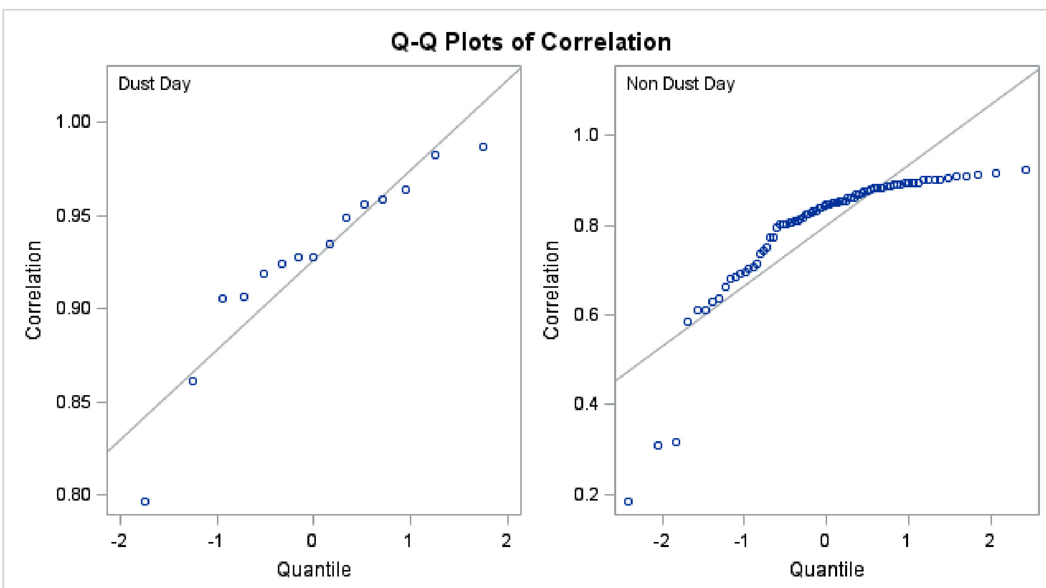

Q-Q Plots of Correlation
Dust Day
Non Dust Day
Correlation
Quantile

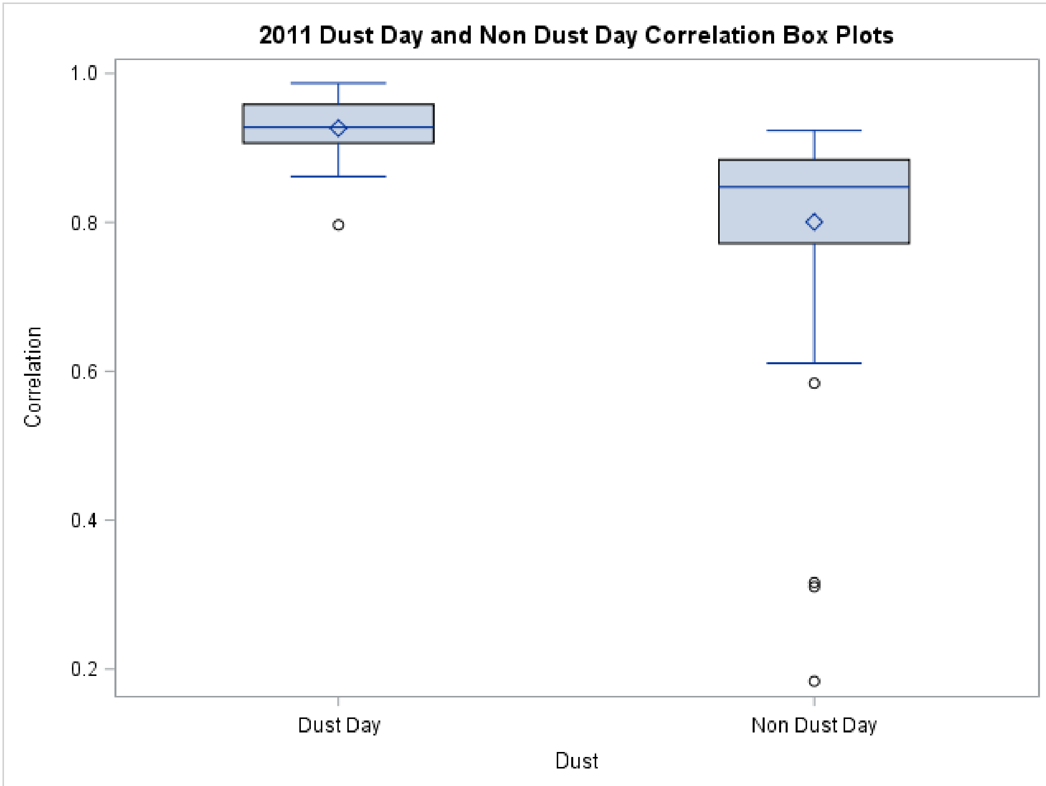
2011 Dust Day and Non Dust Day Correlation Box Plots
1.0
0.8
0.6
0.4
0.2
Correlation
Dust Day
Non Dust Day
Dust

2012 Dust Day and Non Dust Day Ttest

The TTEST Procedure

Variable: Correlation (Correlation)

Dust	N	Mean	Std Dev	Std Err	Minimum	Maximum
Dust Day	19	0.8769	0.0852	0.0195	0.6971	0.9770
Non Dust Day	64	0.7114	0.1697	0.0212	0.2631	0.9459
Diff (1-2)		0.1656	0.1550	0.0405		

Dust	Method	Mean	95% CL Mean		Std Dev	95% CL Std Dev	
Dust Day		0.8769	0.8359	0.9180	0.0852	0.0644	0.1259
Non Dust Day		0.7114	0.6690	0.7538	0.1697	0.1446	0.2056
Diff (1-2)	**Pooled**	0.1656	0.0850	0.2461	0.1550	0.1344	0.1832
Diff (1-2)	**Satterthwaite**	0.1656	0.1079	0.2232			

Method	Variances	DF	t Value	Pr > |t|
Pooled	Equal	81	4.09	0.0001
Satterthwaite	Unequal	61.176	5.74	<.0001

Equality of Variances

Method	Num DF	Den DF	F Value	Pr > F
Folded F	63	18	3.97	0.0020

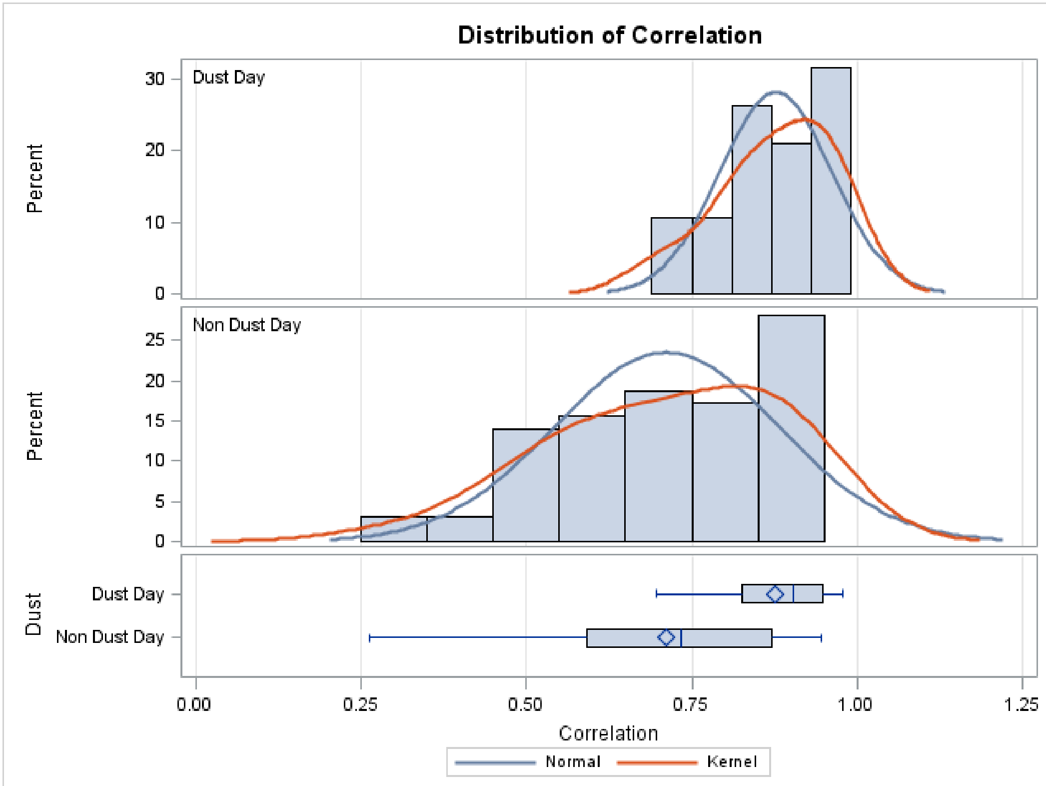
Distribution of Correlation
Dust Day
Non Dust Day
Percent
Dust
Correlation
Normal
Kernel

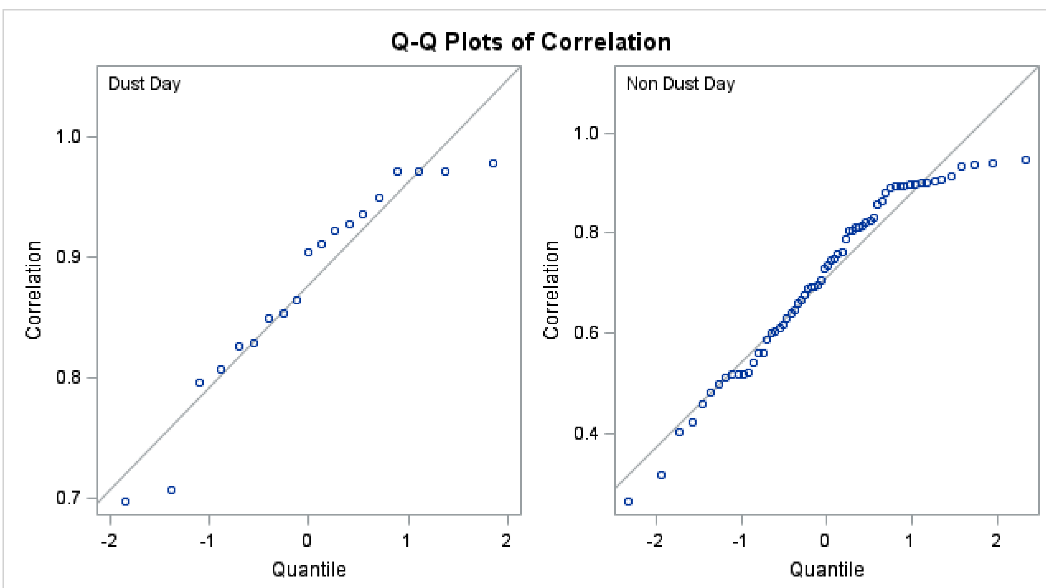
Q-Q Plots of Correlation
Dust Day
Non Dust Day
Correlation
Quantile

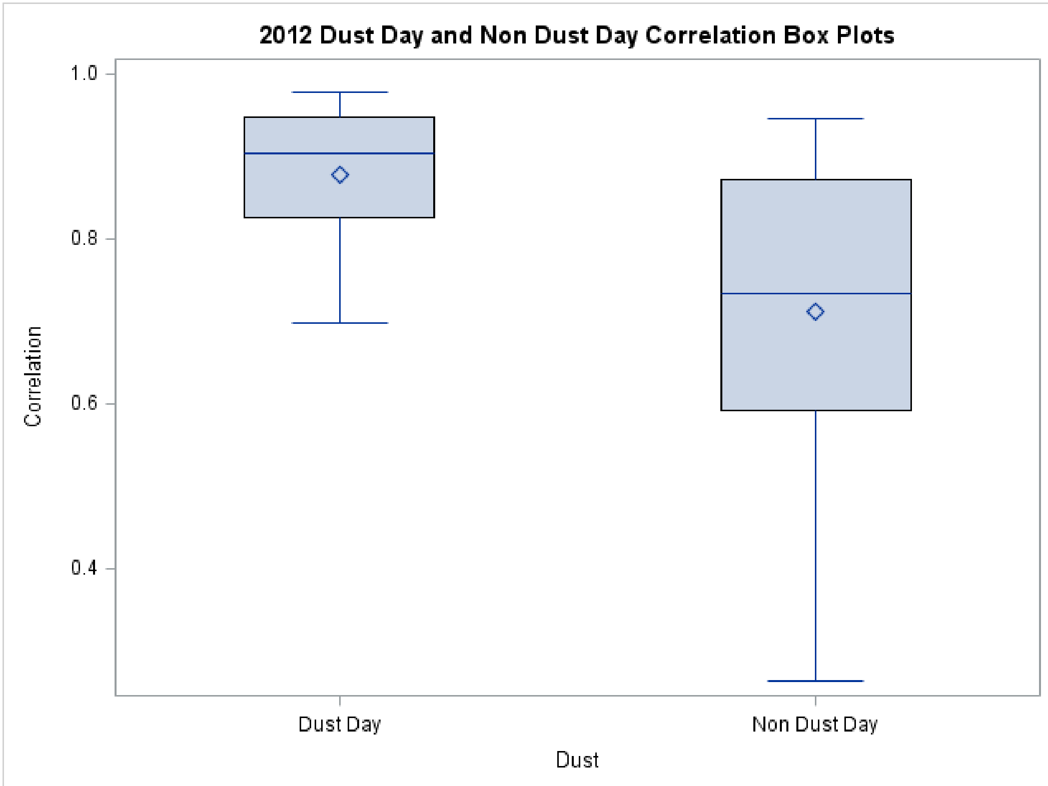
2012 Dust Day and Non Dust Day Correlation Box Plots
1.0
0.8
0.6
0.4
Correlation
Dust Day
Non Dust Day
Dust

2013 Dust Day and Non Dust Day Ttest

The TTEST Procedure

Variable: Correlation (Correlation)

Dust	N	Mean	Std Dev	Std Err	Minimum	Maximum
Dust Day	16	0.9208	0.0294	0.00735	0.8707	0.9690
Non Dust Day	72	0.7645	0.1284	0.0151	0.3580	0.9554
Diff (1-2)		0.1563	0.1173	0.0324		

Dust	Method	Mean	95% CL Mean		Std Dev	95% CL Std Dev	
Dust Day		0.9208	0.9051	0.9365	0.0294	0.0217	0.0455
Non Dust Day		0.7645	0.7344	0.7947	0.1284	0.1103	0.1536
Diff (1-2)	**Pooled**	0.1563	0.0919	0.2207	0.1173	0.1021	0.1378
Diff (1-2)	**Satterthwaite**	0.1563	0.1228	0.1897			

Method	Variances	DF	t Value	Pr > |t|
Pooled	Equal	86	4.82	<.0001
Satterthwaite	Unequal	85.834	9.29	<.0001

Equality of Variances

Method	Num DF	Den DF	F Value	Pr > F
Folded F	71	15	19.05	<.0001

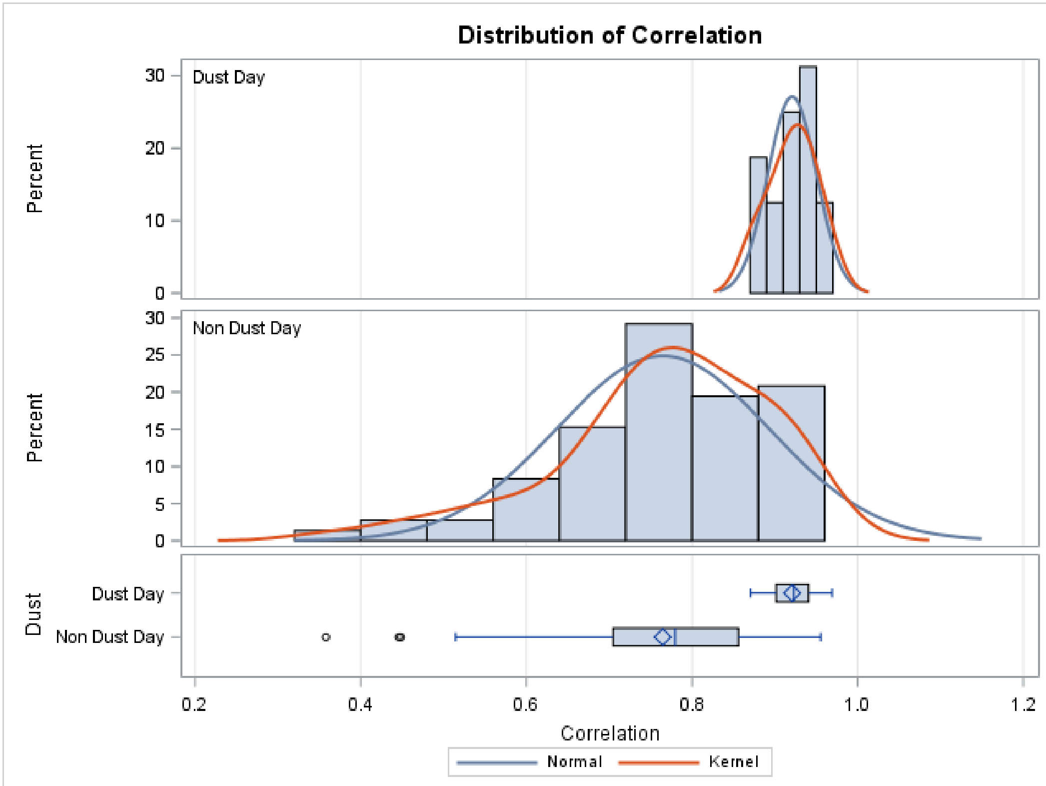

Distribution of Correlation
Dust Day
Non Dust Day
Percent
Percent
Dust
Dust Day
Non Dust Day
Correlation
Normal
Kernel

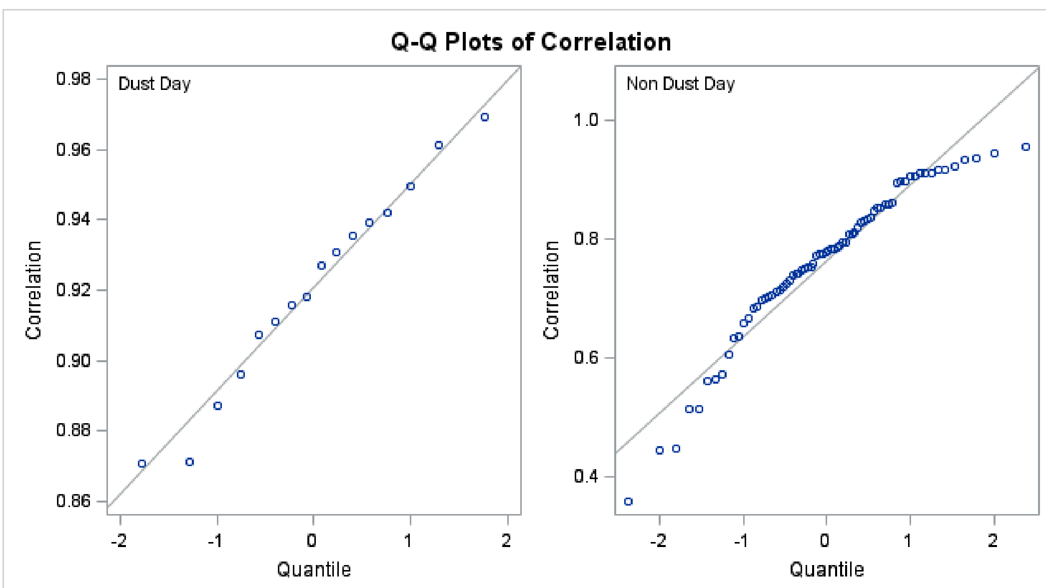

Q-Q Plots of Correlation
Dust Day
Non Dust Day
Correlation
Correlation
Quantile
Quantile

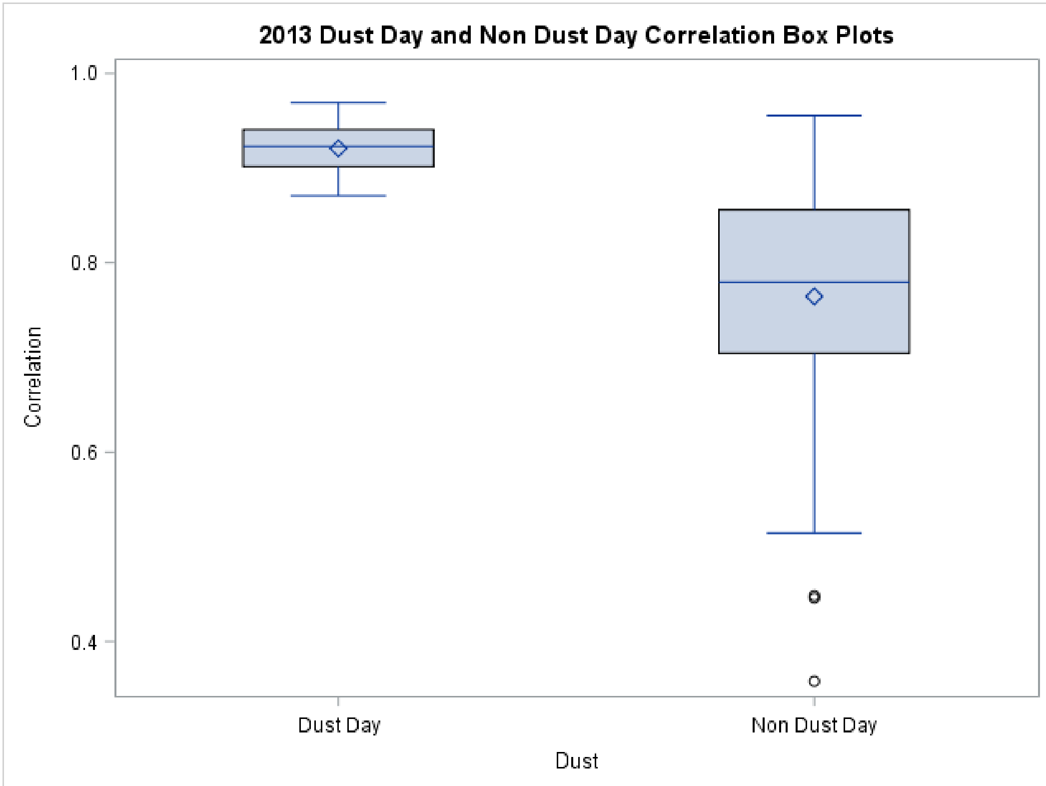
2013 Dust Day and Non Dust Day Correlation Box Plots
1.0
0.8
0.6
0.4
Correlation
Dust Day
Non Dust Day
Dust

2014 Dust Day and Non Dust Day Ttest

The TTEST Procedure

Variable: Correlation (Correlation)

Dust	N	Mean	Std Dev	Std Err	Minimum	Maximum
Dust Day	10	0.9221	0.0533	0.0169	0.8058	0.9755
Non Dust Day	77	0.7631	0.1591	0.0181	0.3251	0.9447
Diff (1-2)		0.1590	0.1515	0.0509		

Dust	Method	Mean	95% CL Mean		Std Dev	95% CL Std Dev	
Dust Day		0.9221	0.8840	0.9602	0.0533	0.0367	0.0973
Non Dust Day		0.7631	0.7270	0.7992	0.1591	0.1374	0.1892
Diff (1-2)	**Pooled**	0.1590	0.0577	0.2602	0.1515	0.1317	0.1782
Diff (1-2)	**Satterthwaite**	0.1590	0.1088	0.2092			

Method	Variances	DF	t Value	Pr > |t|
Pooled	Equal	85	3.12	0.0025
Satterthwaite	Unequal	36.159	6.42	<.0001

Equality of Variances

Method	Num DF	Den DF	F Value	Pr > F
Folded F	76	9	8.91	0.0014

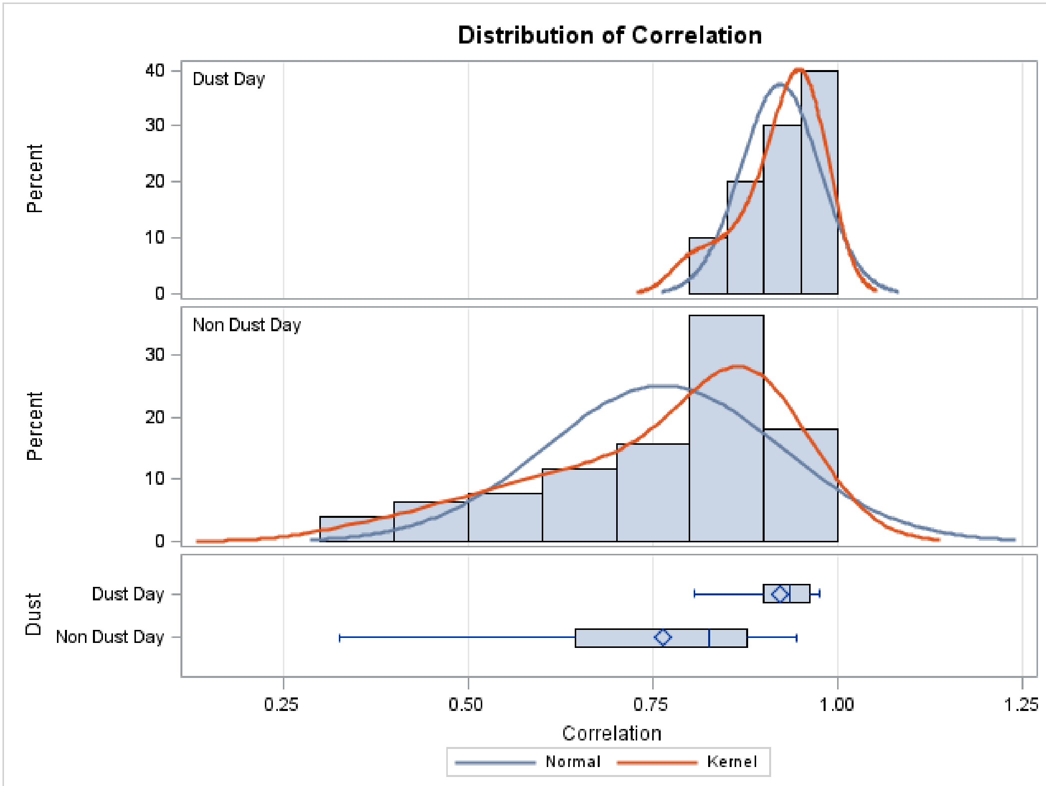
Distribution of Correlation
Dust Day
Non Dust Day
Percent
Dust
Correlation
Normal
Kernel

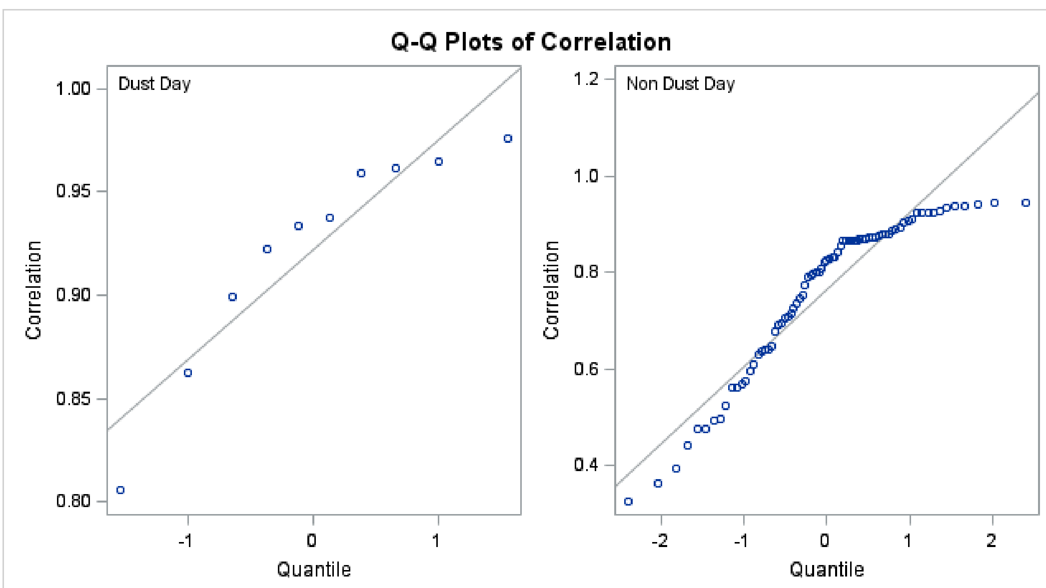
Q-Q Plots of Correlation
Dust Day
Non Dust Day
Correlation
Quantile

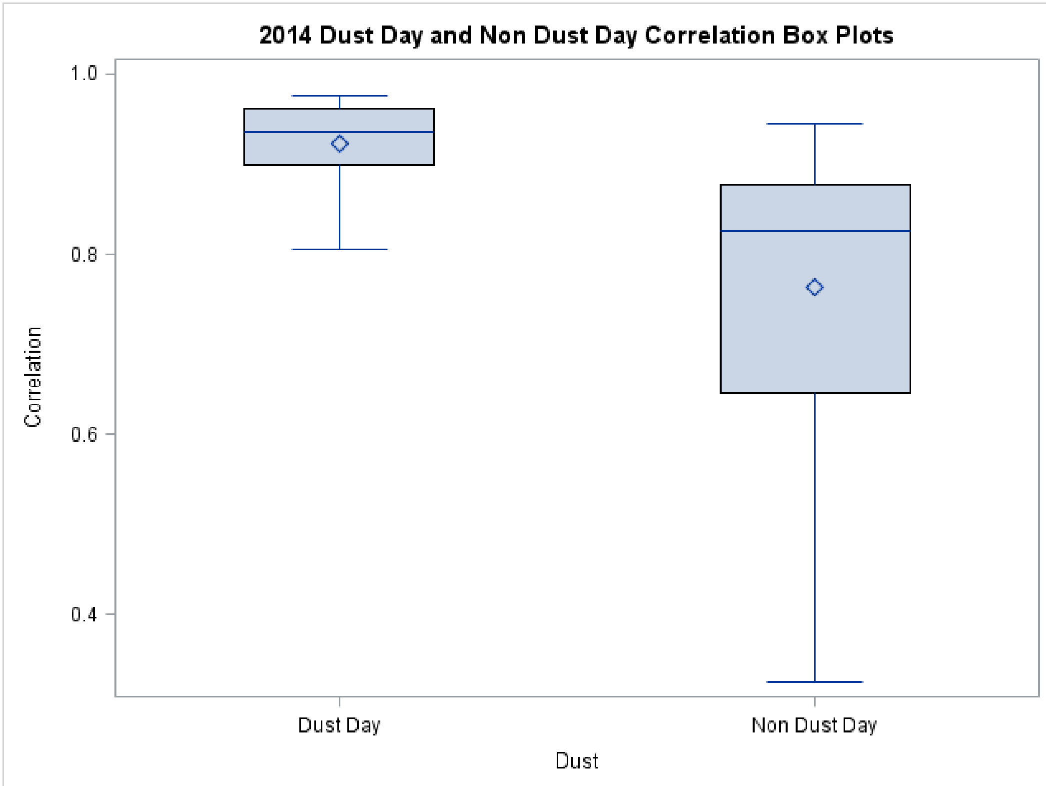
2014 Dust Day and Non Dust Day Correlation Box Plots
1.0
0.8
0.6
0.4
Correlation
Dust Day
Non Dust Day
Dust

D.2 UNIVARIATE:

The SAS code that was used to generate the following UNIVARIATE results:

```
proc import
      out = dust
      datafile =
'H:\500dust_days\Cross_correlations/2011_Normal_Test/2012_SAS'
      replace
      dbms = xlsx;
      run;

proc print data = dust;
      run;

proc univariate data = dust normal;
      class dust;
      var correlation;
      qqplot correlation /Normal(mu=est sigma=est color=red l=1);
      Title "2012 Dust Day and Non Dust Day Correlation QQ Plots";
      run;

proc sgplot data = dust;
      vbox correlation / category = dust;
      Title "2012 Dust Day and Non Dust Day Correlation Box Plots";
      run;
```

SAS UNIVARIATE Results

2011 Dust Day and Non Dust Day Correlation Box Plots

The UNIVARIATE Procedure
Variable: Correlation (Correlation)
Dust = Dust Day

Moments

N	19	**Sum Weights**	19
Mean	0.87693657	**Sum Observations**	16.6617948
Std Deviation	0.08516773	**Variance**	0.00725354
Skewness	-0.7668017	**Kurtosis**	-0.1123167
Uncorrected SS	14.741901	**Corrected SS**	0.13056377
Coeff Variation	9.71196065	**Std Error Mean**	0.01953882

Basic Statistical Measures

Location		Variability	
Mean	0.876937	**Std Deviation**	0.08517
Median	0.904383	**Variance**	0.00725
Mode	.	**Range**	0.27991
		Interquartile Range	0.12232

Tests for Location: Mu0=0

Test	Statistic		p Value	
Student's t	**t**	44.88176	**Pr > |t|**	<.0001
Sign	**M**	9.5	**Pr >= |M|**	<.0001
Signed Rank	**S**	95	**Pr >= |S|**	<.0001

Tests for Normality

Test	Statistic		p Value	
Shapiro-Wilk	**W**	0.91192	**Pr < W**	0.0803
Kolmogorov-Smirnov	**D**	0.152688	**Pr > D**	>0.1500
Cramer-von Mises	**W-Sq**	0.068385	**Pr > W-Sq**	>0.2500

Tests for Normality

Test		Statistic		p Value
Anderson-Darling	**A-Sq**	0.514315	**Pr > A-Sq**	0.1755

Quantiles (Definition 5)

Level	Quantile
100% Max	0.976990
99%	0.976990
95%	0.976990
90%	0.970658
75% Q3	0.948344
50% Median	0.904383
25% Q1	0.826028
10%	0.706807
5%	0.697080
1%	0.697080
0% Min	0.697080

Extreme Observations

Lowest		Highest	
Value	**Obs**	**Value**	**Obs**
0.697080	71	0.948344	81
0.706807	66	0.970083	65
0.795046	69	0.970658	78
0.806538	73	0.970658	77
0.826028	83	0.976990	67

2011 Dust Day and Non Dust Day Correlation Box Plots

The UNIVARIATE Procedure
Variable: Correlation (Correlation)
Dust = Non Dust Day

Moments

N	79	**Sum Weights**	79
Mean	0.80041872	**Sum Observations**	63.2330788
Std Deviation	0.13528935	**Variance**	0.01830321
Skewness	-2.5662993	**Kurtosis**	7.92391209
Uncorrected SS	52.0405903	**Corrected SS**	1.42765034
Coeff Variation	16.9023226	**Std Error Mean**	0.01522124

Basic Statistical Measures

Location		**Variability**	
Mean	0.800419	**Std Deviation**	0.13529
Median	0.847416	**Variance**	0.01830
Mode	.	**Range**	0.73935
		Interquartile Range	0.11251

Tests for Location: Mu0=0

Test	**Statistic**		**p Value**	
Student's t	**t**	52.58564	**Pr > |t|**	<.0001
Sign	**M**	39.5	**Pr >= |M|**	<.0001
Signed Rank	**S**	1580	**Pr >= |S|**	<.0001

Tests for Normality

Test	**Statistic**		**p Value**	
Shapiro-Wilk	**W**	0.718345	**Pr < W**	<0.0001
Kolmogorov-Smirnov	**D**	0.22724	**Pr > D**	<0.0100
Cramer-von Mises	**W-Sq**	1.074796	**Pr > W-Sq**	<0.0050
Anderson-Darling	**A-Sq**	6.117582	**Pr > A-Sq**	<0.0050

Quantiles (Definition 5)

Level	**Quantile**

Quantiles (Definition 5)

Level	Quantile
100% Max	0.923107
99%	0.923107
95%	0.908688
90%	0.902036
75% Q3	0.884136
50% Median	0.847416
25% Q1	0.771623
10%	0.638734
5%	0.583856
1%	0.183757
0% Min	0.183757

Extreme Observations

Lowest		**Highest**	
Value	**Obs**	**Value**	**Obs**
0.183757	33	0.908642	51
0.310587	34	0.908688	66
0.316177	26	0.914088	8
0.583856	27	0.916718	47
0.610728	23	0.923107	52

2011 Dust Day and Non Dust Day Correlation Box Plots

The UNIVARIATE Procedure

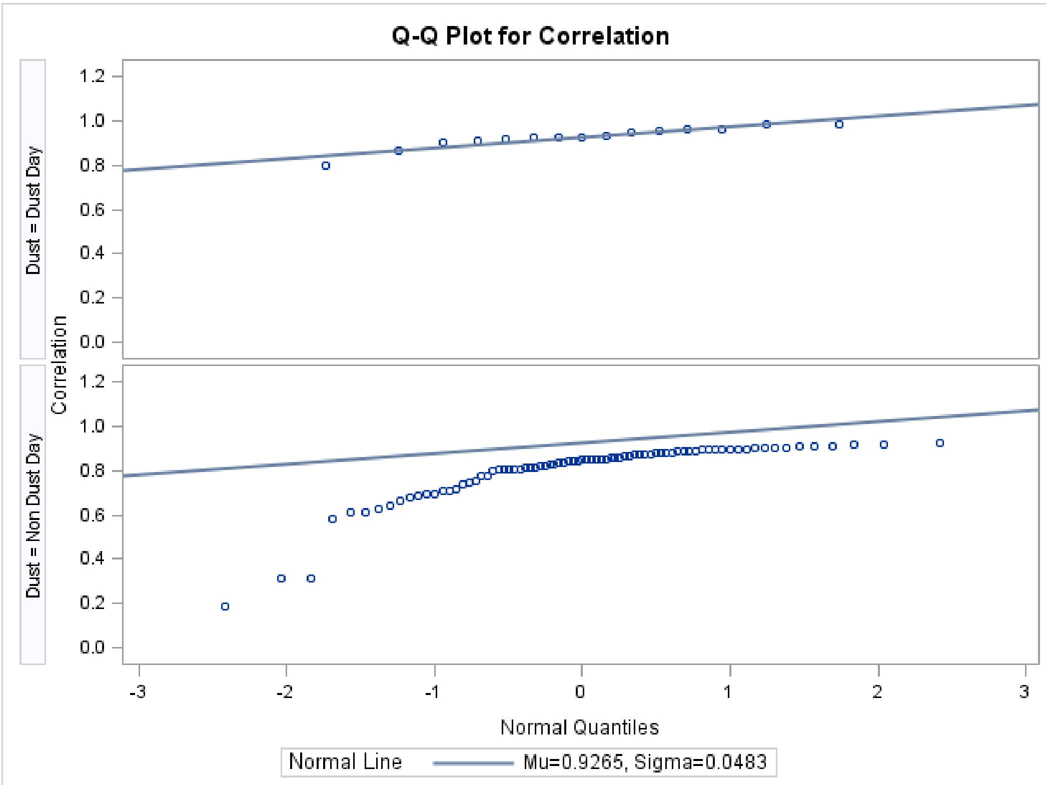

2012 Dust Day and Non Dust Day Correlation QQ Plots

The UNIVARIATE Procedure
Variable: Correlation (Correlation)
Dust = Dust Day

Moments

N	19	**Sum Weights**	19
Mean	0.87693657	**Sum Observations**	16.6617948

Moments

Std Deviation	0.08516773	**Variance**	0.00725354
Skewness	-0.7668017	**Kurtosis**	-0.1123167
Uncorrected SS	14.741901	**Corrected SS**	0.13056377
Coeff Variation	9.71196065	**Std Error Mean**	0.01953882

Basic Statistical Measures

Location		Variability	
Mean	0.876937	**Std Deviation**	0.08517
Median	0.904383	**Variance**	0.00725
Mode	.	**Range**	0.27991
		Interquartile Range	0.12232

Tests for Location: Mu0=0

Test	Statistic		p Value	
Student's t	**t**	44.88176	**Pr > |t|**	<.0001
Sign	**M**	9.5	**Pr >= |M|**	<.0001
Signed Rank	**S**	95	**Pr >= |S|**	<.0001

Tests for Normality

Test	Statistic		p Value	
Shapiro-Wilk	**W**	0.91192	**Pr < W**	0.0803
Kolmogorov-Smirnov	**D**	0.152688	**Pr > D**	>0.1500
Cramer-von Mises	**W-Sq**	0.068385	**Pr > W-Sq**	>0.2500
Anderson-Darling	**A-Sq**	0.514315	**Pr > A-Sq**	0.1755

Quantiles (Definition 5)

Level	Quantile
100% Max	0.976990
99%	0.976990

Quantiles (Definition 5)

Level	Quantile
95%	0.976990
90%	0.970658
75% Q3	0.948344
50% Median	0.904383
25% Q1	0.826028
10%	0.706807
5%	0.697080
1%	0.697080
0% Min	0.697080

Extreme Observations

Lowest		Highest	
Value	**Obs**	**Value**	**Obs**
0.697080	71	0.948344	81
0.706807	66	0.970083	65
0.795046	69	0.970658	78
0.806538	73	0.970658	77
0.826028	83	0.976990	67

The UNIVARIATE Procedure
Variable: Correlation (Correlation)
Dust = Non Dust Day

Moments

N	64	**Sum Weights**	64
Mean	0.71138177	**Sum Observations**	45.5284331
Std Deviation	0.16973854	**Variance**	0.02881117
Skewness	-0.5320064	**Kurtosis**	-0.473839
Uncorrected SS	34.203201	**Corrected SS**	1.81510387
Coeff Variation	23.860401	**Std Error Mean**	0.02121732

Basic Statistical Measures

Location		Variability	
Mean	0.711382	**Std Deviation**	0.16974
Median	0.733048	**Variance**	0.02881
Mode	.	**Range**	0.68281
		Interquartile Range	0.27943

Tests for Location: Mu0=0

Test	Statistic		p Value	
Student's t	**t**	33.52836	**Pr > |t|**	<.0001
Sign	**M**	32	**Pr >= |M|**	<.0001
Signed Rank	**S**	1040	**Pr >= |S|**	<.0001

Tests for Normality

Test	Statistic		p Value	
Shapiro-Wilk	**W**	0.945367	**Pr < W**	0.0068
Kolmogorov-Smirnov	**D**	0.111625	**Pr > D**	0.0464
Cramer-von Mises	**W-Sq**	0.135756	**Pr > W-Sq**	0.0377

Tests for Normality

Test		Statistic		p Value
Anderson-Darling	**A-Sq**	0.966372	**Pr > A-Sq**	0.0153

Quantiles (Definition 5)

Level	Quantile
100% Max	0.945870
99%	0.945870
95%	0.934653
90%	0.904867
75% Q3	0.871719
50% Median	0.733048
25% Q1	0.592288
10%	0.499272
5%	0.422915
1%	0.263058
0% Min	0.263058

Extreme Observations

Lowest		Highest	
Value	**Obs**	**Value**	**Obs**
0.263058	8	0.912725	24
0.315680	3	0.934653	35
0.401980	17	0.935533	23
0.422915	32	0.938226	41
0.459152	54	0.945870	22

2012 Dust Day and Non Dust Day Correlation QQ Plots

The UNIVARIATE Procedure

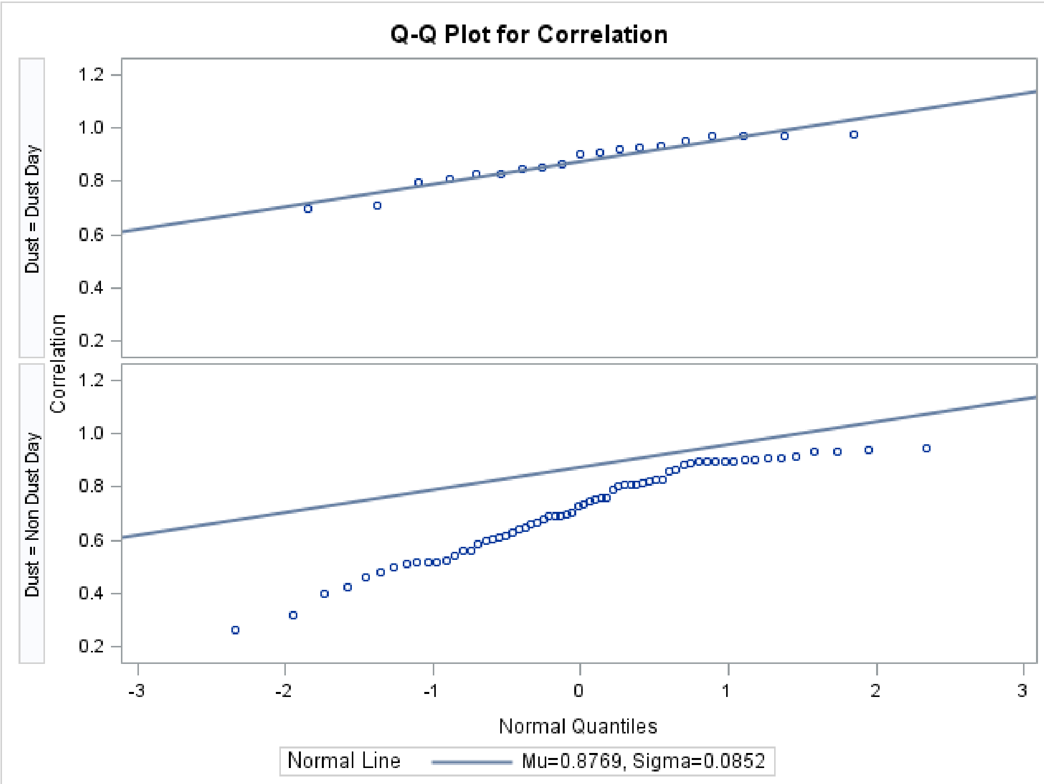

2013 Dust Day and Non Dust Day Correlation QQ Plots

The UNIVARIATE Procedure
Variable: Correlation (Correlation)
Dust = Dust Day

Moments

N	16	**Sum Weights**	16
Mean	0.92079434	**Sum Observations**	14.7327094

Moments

Std Deviation	0.02940862	**Variance**	0.00086487
Skewness	-0.2404881	**Kurtosis**	-0.6138389
Uncorrected SS	13.5787684	**Corrected SS**	0.01297301
Coeff Variation	3.19383174	**Std Error Mean**	0.00735216

Basic Statistical Measures

Location		**Variability**	
Mean	0.920794	**Std Deviation**	0.02941
Median	0.922797	**Variance**	0.0008649
Mode	.	**Range**	0.09832
		Interquartile Range	0.03894

Tests for Location: Mu0=0

Test	**Statistic**		**p Value**	
Student's t	**t**	125.2414	**Pr > |t|**	<.0001
Sign	**M**	8	**Pr >= |M|**	<.0001
Signed Rank	**S**	68	**Pr >= |S|**	<.0001

Tests for Normality

Test	**Statistic**		**p Value**	
Shapiro-Wilk	**W**	0.970217	**Pr < W**	0.8421
Kolmogorov-Smirnov	**D**	0.087213	**Pr > D**	>0.1500
Cramer-von Mises	**W-Sq**	0.019175	**Pr > W-Sq**	>0.2500
Anderson-Darling	**A-Sq**	0.1604	**Pr > A-Sq**	>0.2500

Quantiles (Definition 5)

Level	**Quantile**
100% Max	0.969028
99%	0.969028

Quantiles (Definition 5)

Level	Quantile
95%	0.969028
90%	0.961461
75% Q3	0.940545
50% Median	0.922797
25% Q1	0.901601
10%	0.871215
5%	0.870711
1%	0.870711
0% Min	0.870711

Extreme Observations

Lowest		Highest	
Value	**Obs**	**Value**	**Obs**
0.870711	87	0.939004	82
0.871215	81	0.942086	79
0.887301	75	0.949679	80
0.895924	73	0.961461	77
0.907278	84	0.969028	85

The UNIVARIATE Procedure
Variable: Correlation (Correlation)
Dust = Non Dust Day

Moments

N	72	**Sum Weights**	72
Mean	0.76451344	**Sum Observations**	55.044968
Std Deviation	0.1283513	**Variance**	0.01647406
Skewness	-0.9313137	**Kurtosis**	0.8838301
Uncorrected SS	43.2522761	**Corrected SS**	1.16965803
Coeff Variation	16.7886259	**Std Error Mean**	0.01512635

Basic Statistical Measures

Location		**Variability**	
Mean	0.764513	**Std Deviation**	0.12835
Median	0.779575	**Variance**	0.01647
Mode	0.898523	**Range**	0.59733
		Interquartile Range	0.15133

Tests for Location: Mu0=0

Test	**Statistic**		**p Value**	
Student's t	**t**	50.54185	**Pr > |t|**	<.0001
Sign	**M**	36	**Pr >= |M|**	<.0001
Signed Rank	**S**	1314	**Pr >= |S|**	<.0001

Tests for Normality

Test	**Statistic**		**p Value**	
Shapiro-Wilk	**W**	0.937779	**Pr < W**	0.0015
Kolmogorov-Smirnov	**D**	0.09281	**Pr > D**	0.1263
Cramer-von Mises	**W-Sq**	0.147351	**Pr > W-Sq**	0.0248

Tests for Normality

Test	Statistic		p Value	
Anderson-Darling	**A-Sq**	1.075458	**Pr > A-Sq**	0.0079

Quantiles (Definition 5)

Level	Quantile
100% Max	0.955352
99%	0.955352
95%	0.934536
90%	0.912211
75% Q3	0.855889
50% Median	0.779575
25% Q1	0.704555
10%	0.572685
5%	0.514621
1%	0.358025
0% Min	0.358025

Extreme Observations

Lowest		Highest	
Value	**Obs**	**Value**	**Obs**
0.358025	63	0.923583	72
0.445888	9	0.934536	52
0.448454	16	0.937849	32
0.514621	40	0.945025	25
0.514833	35	0.955352	6

2013 Dust Day and Non Dust Day Correlation QQ Plots

The UNIVARIATE Procedure

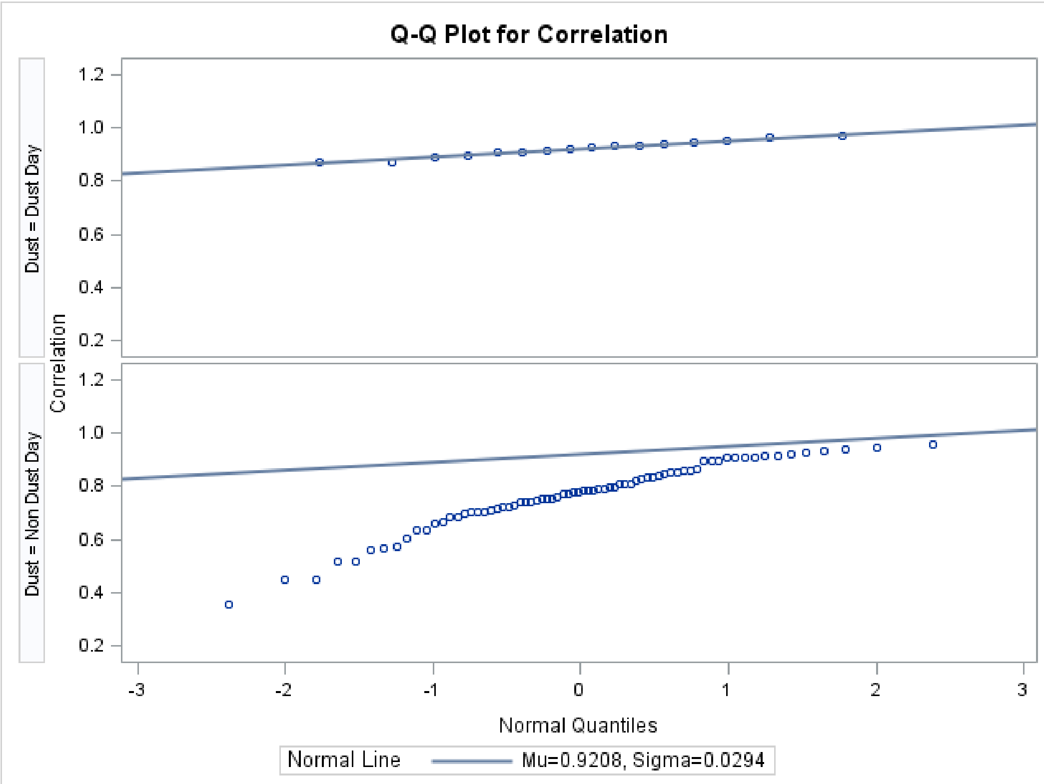

2014 Dust Day and Non Dust Day Correlation QQ Plots

The UNIVARIATE Procedure
Variable: Correlation (Correlation)
Dust = Dust Day

Moments

N	10	**Sum Weights**	10
Mean	0.92209033	**Sum Observations**	9.22090326

Moments

Std Deviation	0.05329758	**Variance**	0.00284063
Skewness	-1.3349949	**Kurtosis**	1.39012753
Uncorrected SS	8.52807138	**Corrected SS**	0.02556569
Coeff Variation	5.78008233	**Std Error Mean**	0.01685417

Basic Statistical Measures

Location		**Variability**	
Mean	0.922090	**Std Deviation**	0.05330
Median	0.935648	**Variance**	0.00284
Mode	.	**Range**	0.16974
		Interquartile Range	0.06272

Tests for Location: Mu0=0

Test	**Statistic**		**p Value**	
Student's t	**t**	54.70991	**Pr > |t|**	<.0001
Sign	**M**	5	**Pr >= |M|**	0.0020
Signed Rank	**S**	27.5	**Pr >= |S|**	0.0020

Tests for Normality

Test	**Statistic**		**p Value**	
Shapiro-Wilk	**W**	0.868325	**Pr < W**	0.0956
Kolmogorov-Smirnov	**D**	0.200901	**Pr > D**	>0.1500
Cramer-von Mises	**W-Sq**	0.089772	**Pr > W-Sq**	0.1375
Anderson-Darling	**A-Sq**	0.550422	**Pr > A-Sq**	0.1192

Quantiles (Definition 5)

Level	**Quantile**
100% Max	0.975491
99%	0.975491

Quantiles (Definition 5)

Level	Quantile
95%	0.975491
90%	0.969853
75% Q3	0.961592
50% Median	0.935648
25% Q1	0.898872
10%	0.834075
5%	0.805754
1%	0.805754
0% Min	0.805754

Extreme Observations

Lowest		Highest	
Value	**Obs**	**Value**	**Obs**
0.805754	78	0.937484	87
0.862395	84	0.959076	82
0.898872	83	0.961592	81
0.922211	85	0.964216	80
0.933812	86	0.975491	79

The UNIVARIATE Procedure
Variable: Correlation (Correlation)
Dust = Non Dust Day

Moments

N	77	**Sum Weights**	77
Mean	0.76312923	**Sum Observations**	58.7609511
Std Deviation	0.15912151	**Variance**	0.02531965
Skewness	-0.9784742	**Kurtosis**	0.02553981
Uncorrected SS	46.7664933	**Corrected SS**	1.92429369
Coeff Variation	20.8511873	**Std Error Mean**	0.01813358

Basic Statistical Measures

Location		Variability	
Mean	0.763129	**Std Deviation**	0.15912
Median	0.825182	**Variance**	0.02532
Mode	.	**Range**	0.61966
		Interquartile Range	0.23260

Tests for Location: Mu0=0

Test	Statistic		p Value	
Student's t	**t**	42.08376	**Pr > |t|**	<.0001
Sign	**M**	38.5	**Pr >= |M|**	<.0001
Signed Rank	**S**	1501.5	**Pr >= |S|**	<.0001

Tests for Normality

Test	Statistic		p Value	
Shapiro-Wilk	**W**	0.884889	**Pr < W**	<0.0001
Kolmogorov-Smirnov	**D**	0.167528	**Pr > D**	<0.0100
Cramer-von Mises	**W-Sq**	0.544026	**Pr > W-Sq**	<0.0050

Tests for Normality

Test	Statistic		p Value	
Anderson-Darling	A-Sq	3.097913	Pr > A-Sq	<0.0050

Quantiles (Definition 5)

Level	Quantile
100% Max	0.944737
99%	0.944737
95%	0.938142
90%	0.924920
75% Q3	0.877873
50% Median	0.825182
25% Q1	0.645271
10%	0.495769
5%	0.440568
1%	0.325074
0% Min	0.325074

Extreme Observations

Lowest		Highest	
Value	Obs	Value	Obs
0.325074	10	0.935292	54
0.362212	11	0.938142	24
0.393517	12	0.940192	57
0.440568	71	0.944424	53
0.474671	72	0.944737	25

2014 Dust Day and Non Dust Day Correlation QQ Plots

The UNIVARIATE Procedure

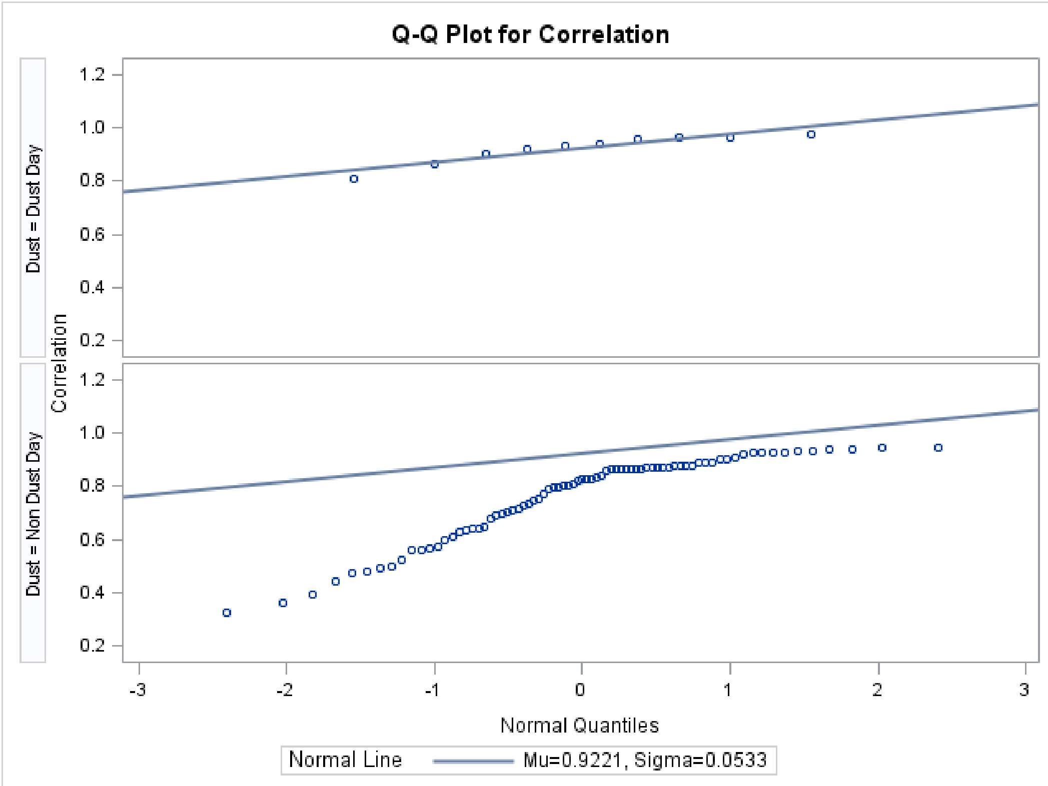

D.3 NPAR1WAY

The SAS code that was used to generate the following NPAR1WAY results:

```
proc import
      out = dust
      datafile = 'H:\500dust_days\Cross_correlations\2011_SAS.xlsx'
      replace
      dbms = xlsx;
      run;

proc print data = dust;
run;

PROC NPAR1WAY data= dust wilcoxon;
      Class dust;
      Var correlation;
      Title "2011 NPAR1WAY";
      Exact; *OPTIONAL; Run;
```

SAS NPAR1WAY Results

2011 NPAR1WAY

Obs	A	Correlation	Dust
1		0.90053613	Non Dust Day
2		0.8474930587	Non Dust Day
3		0.873425044	Non Dust Day
4		0.8023587955	Non Dust Day
5		0.774914068	Non Dust Day
6		0.7513062102	Non Dust Day
7		0.8039147032	Non Dust Day
8		0.9140883634	Non Dust Day
9		0.9024927551	Non Dust Day
10		0.876661335	Non Dust Day
11		0.8841363315	Non Dust Day
12		0.8233840612	Non Dust Day
13		0.6859272732	Non Dust Day
14		0.6296385545	Non Dust Day
15		0.6814380342	Non Dust Day
16		0.7716233812	Non Dust Day
17		0.8320910841	Non Dust Day
18		0.8823502279	Non Dust Day
19		0.7050473758	Non Dust Day
20		0.7377208346	Non Dust Day
21		0.8289573538	Non Dust Day
22		0.6962804962	Non Dust Day
23		0.6107279989	Non Dust Day

Obs	A	Correlation	Dust
24		0.8081808851	Non Dust Day
25		0.61177236	Non Dust Day
26		0.3161766192	Non Dust Day
27		0.5838557451	Non Dust Day
28		0.8112549838	Non Dust Day
29		0.9018151784	Non Dust Day
30		0.8609909413	Non Dust Day
31		0.8153876592	Non Dust Day
32		0.6387336487	Non Dust Day
33		0.1837570594	Non Dust Day
34		0.3105872042	Non Dust Day
35		0.7076854456	Non Dust Day
36		0.6923852442	Non Dust Day
37		0.8421721072	Non Dust Day
38		0.802832933	Non Dust Day
39		0.8068471306	Non Dust Day
40		0.8516451264	Non Dust Day
41		0.851110884	Non Dust Day
42		0.8529398049	Non Dust Day
43		0.8540588901	Non Dust Day
44		0.8955357246	Non Dust Day
45		0.8325364793	Non Dust Day
46		0.7422930522	Non Dust Day
47		0.916718254	Non Dust Day
48		0.9073825631	Non Dust Day
49		0.8689006806	Non Dust Day
50		0.8858571635	Non Dust Day

Obs	A	Correlation	Dust
51		0.9086420665	Non Dust Day
52		0.9231067072	Non Dust Day
53		0.8952357876	Non Dust Day
54		0.841371309	Non Dust Day
55		0.8805687474	Non Dust Day
56		0.8911790263	Non Dust Day
57		0.8949089831	Non Dust Day
58		0.8505292092	Non Dust Day
59		0.8607788363	Non Dust Day
60		0.7970394054	Non Dust Day
61		0.8411419203	Non Dust Day
62		0.8110684324	Non Dust Day
63		0.8168514009	Non Dust Day
64		0.8944227306	Non Dust Day
65		0.8907116657	Non Dust Day
66		0.908688014	Non Dust Day
67		0.902035932	Non Dust Day
68		0.8907244544	Non Dust Day
69		0.8601993106	Non Dust Day
70		0.7138014191	Non Dust Day
71		0.6633768781	Non Dust Day
72		0.8865328787	Non Dust Day
73		0.8840177777	Non Dust Day
74		0.8749087667	Non Dust Day
75		0.8258460474	Non Dust Day
76		0.8474161489	Non Dust Day
77		0.8559193372	Non Dust Day

Obs	A	Correlation	Dust
78		0.8699680078	Non Dust Day
79		0.8821604017	Non Dust Day
80		0.9272114751	Dust Day
81		0.9638431254	Dust Day
82		0.9866818682	Dust Day
83		0.9583727741	Dust Day
84		0.9486470256	Dust Day
85		0.7965567472	Dust Day
86		0.9346379923	Dust Day
87		0.9561702358	Dust Day
88		0.9824476035	Dust Day
89		0.923779147	Dust Day
90		0.9186093645	Dust Day
91		0.9063608579	Dust Day
92		0.9275167373	Dust Day
93		0.9051447863	Dust Day
94		0.8614765876	Dust Day

2011 NPAR1WAY

The NPAR1WAY Procedure

Wilcoxon Scores (Rank Sums) for Variable Correlation Classified by Variable Dust

Dust	N	Sum of Scores	Expected Under H0	Std Dev Under H0	Mean Score
Non Dust Day	79	3260.0	3752.50	96.856853	41.265823
Dust Day	15	1205.0	712.50	96.856853	80.333333

Wilcoxon Two-Sample Test	
Statistic (S)	1205.0000
Normal Approximation	
Z	5.0797
One-Sided Pr > Z	<.0001
Two-Sided Pr > |Z|	<.0001
t Approximation	
One-Sided Pr > Z	<.0001
Two-Sided Pr > |Z|	<.0001
Exact Test	
One-Sided Pr >= S	<.0001
Two-Sided Pr >= |S - Mean|	<.0001

Z includes a continuity correction of 0.5.

Kruskal-Wallis Test	
Chi-Square	25.8554

Kruskal-Wallis Test	
DF	1
Pr > Chi-Square	<.0001

2012 NPAR1WAY

Obs	Event	Correlation	Dust
1		0.6098847618	Non Dust Day
2		0.7600037482	Non Dust Day
3		0.3156799473	Non Dust Day
4		0.5985160939	Non Dust Day
5		0.7883984796	Non Dust Day
6		0.8299204795	Non Dust Day
7		0.521649193	Non Dust Day
8		0.2630581632	Non Dust Day
9		0.6307876894	Non Dust Day
10		0.6591830747	Non Dust Day
11		0.5389999574	Non Dust Day
12		0.4819977958	Non Dust Day
13		0.6753723365	Non Dust Day
14		0.7296803824	Non Dust Day
15		0.8243270304	Non Dust Day
16		0.7594806316	Non Dust Day
17		0.4019804551	Non Dust Day
18		0.6664201169	Non Dust Day
19		0.7439320702	Non Dust Day
20		0.5161148858	Non Dust Day
21		0.6897988913	Non Dust Day
22		0.9458696687	Non Dust Day
23		0.9355325313	Non Dust Day
24		0.9127253509	Non Dust Day

Obs	Event	Correlation	Dust
25		0.8098410202	Non Dust Day
26		0.8101861154	Non Dust Day
27		0.805925295	Non Dust Day
28		0.8625966817	Non Dust Day
29		0.8930820793	Non Dust Day
30		0.8030273523	Non Dust Day
31		0.6914667948	Non Dust Day
32		0.4229148802	Non Dust Day
33		0.6033496801	Non Dust Day
34		0.8808417493	Non Dust Day
35		0.9346530841	Non Dust Day
36		0.9048670851	Non Dust Day
37		0.693314556	Non Dust Day
38		0.894077059	Non Dust Day
39		0.9013676208	Non Dust Day
40		0.8913279697	Non Dust Day
41		0.9382262386	Non Dust Day
42		0.8934112706	Non Dust Day
43		0.5601989329	Non Dust Day
44		0.518318703	Non Dust Day
45		0.640134916	Non Dust Day
46		0.7364149231	Non Dust Day
47		0.6162007511	Non Dust Day
48		0.8570324746	Non Dust Day
49		0.8991044784	Non Dust Day
50		0.7497719397	Non Dust Day
51		0.69667899	Non Dust Day

Obs	Event	Correlation	Dust
52		0.8982529208	Non Dust Day
53		0.5102254571	Non Dust Day
54		0.4591516104	Non Dust Day
55		0.5172127995	Non Dust Day
56		0.7042816275	Non Dust Day
57		0.9077124993	Non Dust Day
58		0.8977535077	Non Dust Day
59		0.8206068631	Non Dust Day
60		0.5594140745	Non Dust Day
61		0.815474234	Non Dust Day
62		0.6453687758	Non Dust Day
63		0.4992721302	Non Dust Day
64		0.5860602011	Non Dust Day
65		0.970083129	Dust Day
66		0.706806735	Dust Day
67		0.976989799	Dust Day
68		0.828858009	Dust Day
69		0.795046337	Dust Day
70		0.922013472	Dust Day
71		0.697079627	Dust Day
72		0.904382633	Dust Day
73		0.806538255	Dust Day
74		0.852758349	Dust Day
75		0.927449239	Dust Day
76		0.934893665	Dust Day
77		0.970658301	Dust Day
78		0.970657917	Dust Day

Obs	Event	Correlation	Dust
79		0.848621857	Dust Day
80		0.910270076	Dust Day
81		0.948343986	Dust Day
82		0.864315908	Dust Day
83		0.826027546	Dust Day

2012 NPAR1WAY

The NPAR1WAY Procedure

Wilcoxon Scores (Rank Sums) for Variable Correlation Classified by Variable Dust

Dust	N	Sum of Scores	Expected Under H0	Std Dev Under H0	Mean Score
Non Dust Day	64	2310.0	2688.0	92.260501	36.093750
Dust Day	19	1176.0	798.0	92.260501	61.894737

Wilcoxon Two-Sample Test	
Statistic (S)	1176.0000
Normal Approximation	
Z	4.0917
One-Sided Pr > Z	<.0001
Two-Sided Pr > |Z|	<.0001
t Approximation	
One-Sided Pr > Z	<.0001
Two-Sided Pr > |Z|	<.0001
Exact Test	
One-Sided Pr >= S	<.0001
Two-Sided Pr >= |S - Mean|	<.0001

Z includes a continuity correction of 0.5.

Kruskal-Wallis Test	
Chi-Square	16.7862

Kruskal-Wallis Test	
DF	1
Pr > Chi-Square	<.0001

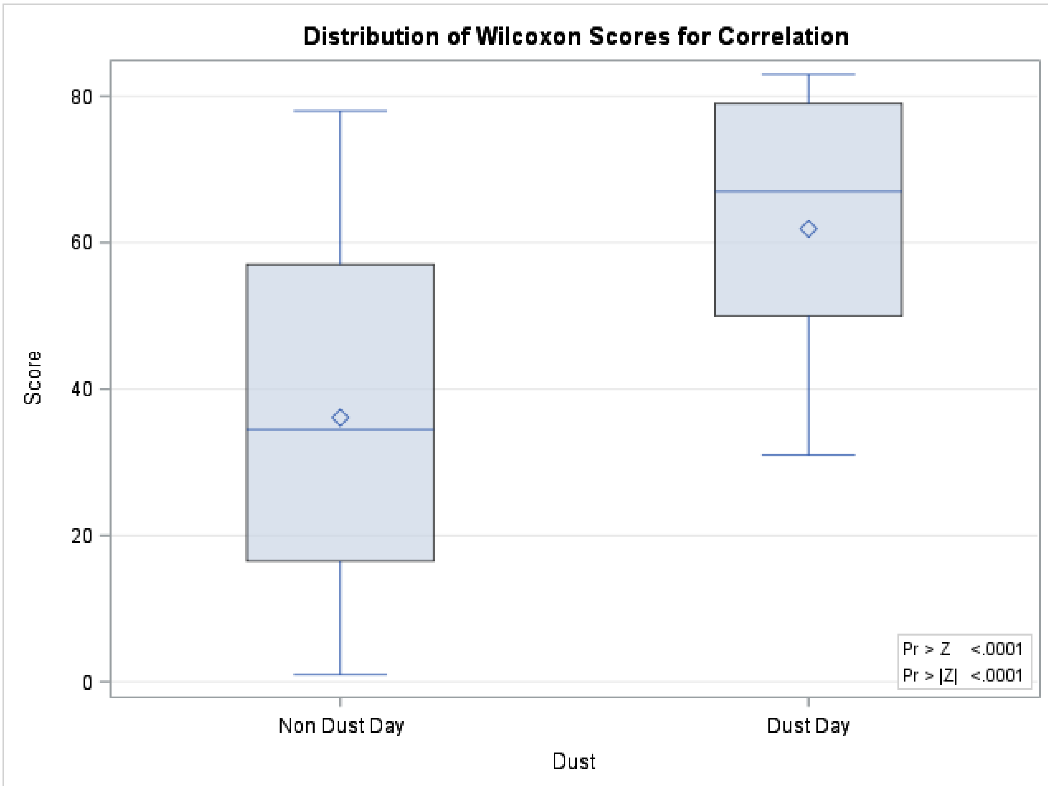

2013 NPAR1WAY

Obs	Event	Correlation	Dust
1		0.7844434304	Non Dust Day
2		0.711418647	Non Dust Day
3		0.7782901652	Non Dust Day
4		0.7542556331	Non Dust Day
5		0.7747689331	Non Dust Day
6		0.955351622	Non Dust Day
7		0.9164706824	Non Dust Day
8		0.6329660317	Non Dust Day
9		0.4458878673	Non Dust Day
10		0.7398819023	Non Dust Day
11		0.8114520868	Non Dust Day
12		0.6865679855	Non Dust Day
13		0.7043316295	Non Dust Day
14		0.6055647893	Non Dust Day
15		0.5726845345	Non Dust Day
16		0.4484541854	Non Dust Day
17		0.7579758096	Non Dust Day
18		0.7197926126	Non Dust Day
19		0.7501235336	Non Dust Day
20		0.853936295	Non Dust Day
21		0.7047782876	Non Dust Day
22		0.906031244	Non Dust Day
23		0.8623700405	Non Dust Day
24		0.7840233668	Non Dust Day

Obs	Event	Correlation	Dust
25		0.9450250502	Non Dust Day
26		0.8098153684	Non Dust Day
27		0.8282596982	Non Dust Day
28		0.7954019172	Non Dust Day
29		0.7882272402	Non Dust Day
30		0.6836575275	Non Dust Day
31		0.7425408071	Non Dust Day
32		0.9378494508	Non Dust Day
33		0.898523279	Non Dust Day
34		0.898523279	Non Dust Day
35		0.5148332709	Non Dust Day
36		0.5621790693	Non Dust Day
37		0.7535212213	Non Dust Day
38		0.713409836	Non Dust Day
39		0.6664439056	Non Dust Day
40		0.5146214293	Non Dust Day
41		0.7296830586	Non Dust Day
42		0.8962353736	Non Dust Day
43		0.8483397825	Non Dust Day
44		0.7808608184	Non Dust Day
45		0.809086383	Non Dust Day
46		0.7871723662	Non Dust Day
47		0.7744317634	Non Dust Day
48		0.9051999342	Non Dust Day
49		0.8347128847	Non Dust Day
50		0.9107451525	Non Dust Day
51		0.910433596	Non Dust Day

Obs	Event	Correlation	Dust
52		0.9345357113	Non Dust Day
53		0.8581163047	Non Dust Day
54		0.794986677	Non Dust Day
55		0.8520994994	Non Dust Day
56		0.7000727265	Non Dust Day
57		0.7423568239	Non Dust Day
58		0.8209590545	Non Dust Day
59		0.8578424378	Non Dust Day
60		0.8320394436	Non Dust Day
61		0.7476736239	Non Dust Day
62		0.5647024496	Non Dust Day
63		0.3580254508	Non Dust Day
64		0.7719804453	Non Dust Day
65		0.636942585	Non Dust Day
66		0.6585649551	Non Dust Day
67		0.6976276863	Non Dust Day
68		0.7242638138	Non Dust Day
69		0.8371390428	Non Dust Day
70		0.9122108068	Non Dust Day
71		0.9176906129	Non Dust Day
72		0.9235830664	Non Dust Day
73		0.8959236231	Dust Day
74		0.9183191567	Dust Day
75		0.8873014904	Dust Day
76		0.9110057942	Dust Day
77		0.9614611672	Dust Day
78		0.9272754701	Dust Day

Obs	**Event**	**Correlation**	**Dust**
79		0.9420863935	Dust Day
80		0.9496788744	Dust Day
81		0.8712151191	Dust Day
82		0.9390041329	Dust Day
83		0.9353662223	Dust Day
84		0.9072781387	Dust Day
85		0.9690281985	Dust Day
86		0.9160184446	Dust Day
87		0.8707109813	Dust Day
88		0.9310362101	Dust Day

2013 NPAR1WAY

The NPAR1WAY Procedure

Wilcoxon Scores (Rank Sums) for Variable Correlation
Classified by Variable Dust

Dust	N	Sum of Scores	Expected Under H0	Std Dev Under H0	Mean Score
Non Dust Day	72	2734.0	3204.0	92.433353	37.972222
Dust Day	16	1182.0	712.0	92.433353	73.875000

Average scores were used for ties.

Wilcoxon Two-Sample Test	
Statistic (S)	1182.0000
Normal Approximation	
Z	5.0793
One-Sided Pr > Z	<.0001
Two-Sided Pr > |Z|	<.0001
t Approximation	
One-Sided Pr > Z	<.0001
Two-Sided Pr > |Z|	<.0001
Exact Test	
One-Sided Pr >= S	<.0001
Two-Sided Pr >= |S - Mean|	<.0001

Z includes a continuity correction of 0.5.

Kruskal-Wallis Test

Kruskal-Wallis Test	
Chi-Square	25.8546
DF	1
Pr > Chi-Square	<.0001

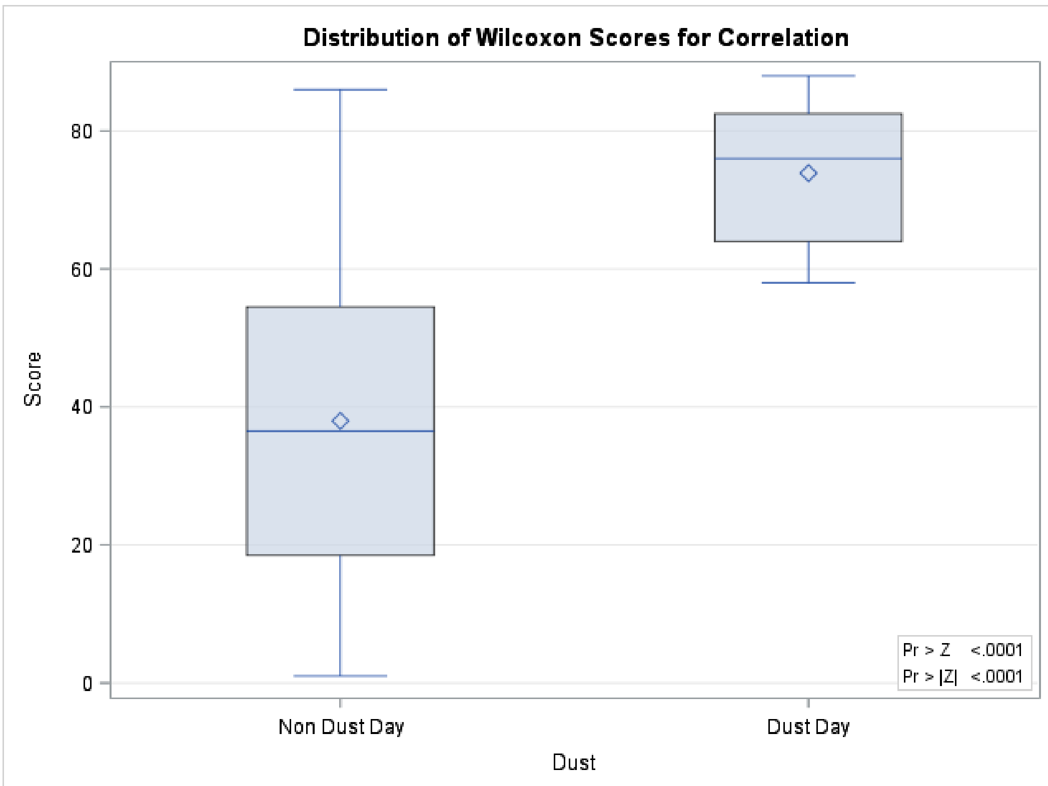

2014 NPAR1WAY

Obs	Event	Correlation	Dust
1		0.5623278523	Non Dust Day
2		0.7968400788	Non Dust Day
3		0.7912450383	Non Dust Day
4		0.5949082094	Non Dust Day
5		0.4917371794	Non Dust Day
6		0.7942870626	Non Dust Day
7		0.8685334298	Non Dust Day
8		0.9046103596	Non Dust Day
9		0.6452705114	Non Dust Day
10		0.3250742721	Non Dust Day
11		0.3622116127	Non Dust Day
12		0.3935172292	Non Dust Day
13		0.4775556693	Non Dust Day
14		0.7046830078	Non Dust Day
15		0.7249489443	Non Dust Day
16		0.5247677118	Non Dust Day
17		0.6363575645	Non Dust Day
18		0.6940246547	Non Dust Day
19		0.6778395975	Non Dust Day
20		0.5748800782	Non Dust Day
21		0.641059438	Non Dust Day
22		0.9235268626	Non Dust Day
23		0.9249196044	Non Dust Day
24		0.938141991	Non Dust Day
25		0.9447369535	Non Dust Day

Obs	Event	Correlation	Dust
26		0.9089149704	Non Dust Day
27		0.8565394978	Non Dust Day
28		0.863680516	Non Dust Day
29		0.8915667694	Non Dust Day
30		0.8060101293	Non Dust Day
31		0.6920303989	Non Dust Day
32		0.7541657904	Non Dust Day
33		0.7136306386	Non Dust Day
34		0.8274332715	Non Dust Day
35		0.9270741452	Non Dust Day
36		0.8715562601	Non Dust Day
37		0.8661823975	Non Dust Day
38		0.9341637576	Non Dust Day
39		0.7999740519	Non Dust Day
40		0.8313197726	Non Dust Day
41		0.870913101	Non Dust Day
42		0.8640579955	Non Dust Day
43		0.8220861053	Non Dust Day
44		0.8251820517	Non Dust Day
45		0.8413474466	Non Dust Day
46		0.9241459185	Non Dust Day
47		0.8650238025	Non Dust Day
48		0.7465292822	Non Dust Day
49		0.8788985324	Non Dust Day
50		0.8903865488	Non Dust Day
51		0.6397222155	Non Dust Day
52		0.5672912092	Non Dust Day

Obs	Event	Correlation	Dust
53		0.9444243459	Non Dust Day
54		0.9352922129	Non Dust Day
55		0.9021950272	Non Dust Day
56		0.736215963	Non Dust Day
57		0.9401916088	Non Dust Day
58		0.7094550565	Non Dust Day
59		0.4957689273	Non Dust Day
60		0.5613539983	Non Dust Day
61		0.8299173007	Non Dust Day
62		0.8744631217	Non Dust Day
63		0.8670164063	Non Dust Day
64		0.8694985273	Non Dust Day
65		0.8662595662	Non Dust Day
66		0.8778730602	Non Dust Day
67		0.8705112692	Non Dust Day
68		0.8864508602	Non Dust Day
69		0.9219959258	Non Dust Day
70		0.6303897663	Non Dust Day
71		0.4405684461	Non Dust Day
72		0.4746707621	Non Dust Day
73		0.6092027065	Non Dust Day
74		0.7723069185	Non Dust Day
75		0.8788578909	Non Dust Day
76		0.866623329	Non Dust Day
77		0.8016165808	Non Dust Day
78		0.8057537694	Dust Day
79		0.9754905251	Dust Day

Obs	Event	Correlation	Dust
80		0.9642157215	Dust Day
81		0.9615924773	Dust Day
82		0.9590761639	Dust Day
83		0.8988719548	Dust Day
84		0.8623952547	Dust Day
85		0.9222106372	Dust Day
86		0.9338124536	Dust Day
87		0.9374843005	Dust Day

2014 NPAR1WAY

The NPAR1WAY Procedure

Wilcoxon Scores (Rank Sums) for Variable Correlation Classified by Variable Dust

Dust	N	Sum of Scores	Expected Under H0	Std Dev Under H0	Mean Score
Non Dust Day	77	3111.0	3388.0	75.144306	40.402597
Dust Day	10	717.0	440.0	75.144306	71.700000

Wilcoxon Two-Sample Test	
Statistic (S)	717.0000
Normal Approximation	
Z	3.6796
One-Sided Pr > Z	0.0001
Two-Sided Pr > |Z|	0.0002
t Approximation	
One-Sided Pr > Z	0.0002
Two-Sided Pr > |Z|	0.0004
Exact Test	
One-Sided Pr >= S	<.0001
Two-Sided Pr >= |S - Mean|	<.0001

Z includes a continuity correction of 0.5.

Kruskal-Wallis Test	
Chi-Square	13.5884

Kruskal-Wallis Test	
DF	1
Pr > Chi-Square	0.0002

REFERENCES

1 Ackerman, S. A. 1997: Remote sensing aerosols using satellite infrared observations. *J. Geophys. Res*, **102(D14)**, 17069–17079, doi:10.1029/96JD03066.

2 Adachi, S., 2007: Climatology of Surface Cyclogenesis and Cyclone Track in East Asia, PhD Dissertation, University of Tsukuba.

3 Al-Dousari, A., and J. Al-Awadhi, 2012: Dust fallout characteristics within global dust storms major trajectories, *Arabian J. Geosciences*, **6**, 3877-3884, doi:10.1007/s1257-012-0644-0.

4 Ashley, W. S., S. Strader, D. Dziubla, and A. Haberlie, 2015: Driving blind: Weather-related vision hazards and fatal motor vehicle crashes. *Bulletin of the American Meteorological Society*, **96**, 755-778.

5 Bernier, S. A., 1995: Climatology of Blowing Dust and Triggering Mechanisms across West Texas. M.S. thesis, Atmospheric Science, Texas Tech University, Lubbock, TX, USA.

6 Brazel, A. and S. Hsu, 1981: The climatology of hazardous Arizona dust storms. *Geological Society of America Special Paper*, **186**, 293-303.

7 Brazel, A. J., and W. G. Nickling, 1986: The relationship of weather types to dust storm generation in Arizona (1965-1980). *International Journal of Climatology*, **6**, 255-275, doi: 10.1002/joc.3370060303.

8 Burritt, B. E. and A. Hyers, 1981: Evaluation of Arizona's highway dust warning system. *Geological Society of America Special Paper*,**186**, 281-292.

9 Bleiweiss, M. P., 2015: Private Communication.

10 Chow, J.C., J.G. Watson, M.C. Green, D.H. Lowenthal, D.W. DuBois, S.D. Kohl, R.T. Egami, J. Gillies, C.F. Rogers, C.A. Frazier and W. Cates, 1999: Middle- and Neighborhood-Scale Variations of PM10 Source Contributions in Las Vegas, Nevada. *Journal of the Air & Waste Management Association*, **49**, No. 6, 641-654.

11 Data Basin, 2016: http://databasin.org/datasets/52d4edfa8cb3445fab79e44939f3109e

12 DuBois, D.W., and E. Ward., 2012: Study If Studies of Fungal Spore Dispersion from Confined Animal Feeding Operations (CAFOs) in FY12 for the Assessment of Land-based Sources of Air Quality Contaminants in the Binational Border Region of Southwestern New Mexico, Northwestern Chihuahua and West Texas. (Accessed December 4, 2015: http://www.wrri.nmsu.edu/publish/otherrpt/Border2012_MaximizingResources/Attachments_Final%20Report_2012%20Part%202/StudyIIe_Fungi_30jun12.pdf)

13 Ekström, M., G.H. McTainsh, and A. Chappell, 2004: Australian dust storms: temporal trends and relationships with synoptic pressure distributions (1960–99). *Int. J. Climatol*, **24**, 1581–1599, doi:10.1002/joc.1072.

14 Ganor, E. Osetinksy, I., A. Stupp, A. Pinhas, 2010: Increasing trend of African dust, over 49 years, in the eastern Mediterranean. *J. Geophysical Research Atmospheres*, **115**, D07201, doi:10.1029/2009JD012500.

15 Gertler, A. W., D. A. Lowenthal, W.G. Coulombe, 1995: PM10 Source Apportionment Study in Bullhead City, Arizona. *Journal of the Air & Waste Management Association*, **45**, 2, 75-82, doi: 10.1080/10473289.1995.10467349.

16 Goudie, A. S., 2009: Dust storms: Recent Developments. *J. Environ Manage*, **90**, 89 – 94.

17 Grineski, S. E., J. G. Staniswalis, P. Bulathsinhala, Y. Peng, and T. E. Gill, 2011: Hospital Admissions for Asthma and Acute Bronchitis in El Paso, Texas: Do Age, Sex, and Insurance Status Modify the Effects of Dust and Low Wind Events? *Environmental Research* **111.8**, 1148-155, doi: 10.1016/j.envres.2011.06.007.

18 Hahnenberger, M. and K. Nicoll, 2012: Meteorological characteristics of dust storm events in the eastern Great Basin of Utah, U.S.A. *Atmospheric Environment*, **60**, 601-612, doi: 10.1016/j.atmosenv.2012.06.029.

19 Hall, F.F., Jr., 1981: Visibility reductions from soil dust in the Western U.S. *Atmo. Environment*, **15**, 1929-1933.

20 Hector, R. F., G. W. Rutherford, C. A. Tsang, L. M. Erhart, O. Mccotter, S. M. Anderson, K. Komatsu, F. Tabnak, D. J. Vugia, Y. Yang, and J. N. Galgiani, 2011: The Public Health Impact of Coccidioidomycosis in Arizona and California. *International Journal of Environmental Research and Public Health,* **8.4**, 1150-173.

21 Holliday, V. T., 1991: The geologic record of wind erosion, eolian deposition, and aridity on the southern High Plains, Great Plains Research. *A Journal of Natural and Social Sciences,* Paper 2.

22 . Karam, B. D., C. Flamant, J. Cuesta, J. Pelon, and E. Williams, 2010: Dust emission and transport associated with a Saharan depression: February 2007 case. *J. Geophys. Res*, **115**, D00H27, doi:10.1029/2009JD012390.

23 Kavouras, I. G., D.W. DuBois, G. Nikolich, and V. Etyemezian, 2015: Monitoring, Source Identification and Health Risks of Air Toxics in Albuquerque, New Mexico, U.S.A.. *Aerosol and Air Quality Research*, 556–571, doi:10.4209/aaqr.2014.04.0075.

24 Kavouras, I.G., V. Etyemezian, D.W. DuBois, J. Xu and M. Pitchford, 2009: Source reconciliation of atmospheric dust causing visibility impairment in Class I areas of the western United States. *Journal of Geophysical Research*, **114**, D02308, doi:10.1029/2008JD009923.

25 Knippertz, P., 2014: Meteorological Aspects of Dust Storms. *Mineral Dust: A Key Player in the Earth System*, P. Knippertz and J.-B. W. Stuut, Eds.,Springer Science+Business Media, 121-147.

26 Kolivras, K. N., P. S. Johnson, A. C. Comrie, and S. R. Yool, 2001: Environmental Variability and Coccidioidomycosis (valley Fever)." *Aerobiologia*, 17, 31-42.

27 Lee, J.A. and T.E. Gill, 2015: Multiple causes of wind erosion in the Dust Bowl. *Aeolian Research*, **19**, 15-36, doi:10.1016/j.aeolia.2015.09.002.

28 Lee, J. A., C. B. Matthew, J. M. Mbongowo, and T. E. Gill., 2012: Geomorphic and Land Cover Characteristics of Aeolian Dust Sources in West Texas and Eastern New Mexico, USA. *Aeolian Research*, **3.4**, 459-66.

29 Leslie, L. M. and Speer, M. S. (2006), Modelling dust transport over central eastern Australia. *Met. Apps*, 13: 141–167. doi:10.1017/S1350482706002155

30 Lewis, R., 1990: *Practical Digital Image Processing*, Ellis Horwood.

31 Mesinger,F., G. DiMego, E. Kalnay, K. Mitchell, P. C. Shafran, W. Ebisuzaki, D. Jović, J. Woollen, E. Rogers, E. H. Berbery, M. B. Ek, Yun Fan, R. Grumbine, W. Higgins, H. Li, Y. Lin, G. Manikin, D. Parrish, and W. Shi, 2006: North American Regional Reanalysis. *Bull. Amer. Meteor. Soc*, **87**, 343–360. doi: http://dx.doi.org/10.1175/BAMS-87-3-343

32 Nickling, W. G., and A. J. Brazel, 1984: Temporal and spatial characteristics of Arizona dust storms (1965-1980). *Journal of Climatology*, **4**, 645-660.

33 Nolen, Barbara, ca. 2003: private communication, Chihuahuan Desert Shapefile downloaded from http://jornada-www.nmsu.edu/GIS/giscat.htm -- site is no longer active.

34 Novlan, 2015: Private communication.

35 Novlan, D.J., M. Hardiman, and T.E. Gill, 2007: A synoptic climatology of blowing dust events in El Paso, Texas from 1932-2005. in 87th AMS Annual Meeting. 87th AMS Annual Meeting, San Antonio, TX, 14-18 January.

36 Offer, Z. Y. and D. Goossens, 2001: Ten years of aeolian dust dynamics in a desert region (Negev desert, Israel): analysis of airborne dust concentration, dust accumulation and the high-magnitude dust events. *Journal of Arid Environments*, **47**, 211-249, doi: 10.1006/jare.200.0706.

37 Orgill, M. M. and G. A. Sehmel, 1976: Frequency and diurnal variation of dust storms in the contiguous U.S.A. *Atmospheric Environment*, **10**, No.10, 813-825.

38 Patterson, E.M. and D.A. Gillette., 1977: Measurements of visibility vs. mass-concentration for airborne soil particles. *Atmos. Environ*, **2**, 193-196.

39 Peterson, F. F., 1981: Landforms of the basin & range province defined for soil survey. Technical. *Bulletin Nevada Agricultural Experimentation*, **28**, 52.

40 Pinto, J.G., Spangehl, T., Ulbrich, U. and Speth, P., 2005: Sensitivities of a cyclone detection and tracking algorithm: individual tracks and climatology. *Meteorologische Zeitschrift*, **14**, No.6, 823-838.

41 Pollard, M. C., 1978: Guidelines for forecasting dust storms in the southern Great Plains. *National Weather Digest*, **3**, No.4, 40-44.

42 Qi, S.L., 2010: Digital map of the aquifer boundary of the High Plains aquifer in parts of Colorado, Kansas, Nebraska, New Mexico, Oklahoma, South Dakota, Texas, and Wyoming. *U.S. Geological Survey Data Series*, **543**.

43 Rivera-Rivera N. I., T. E. Gill, K. A. Gebhart, J. L. Hand, M. P. Bleiweiss, and R. M. Fitzgerald, 2009: Wind Modeling of Chihuahuan Desert Dust Outbreaks. *Atmos. Environ*., **43.2**, 347-54.

44 Rodopoulou, S., M.-C. Chalbot, E. Samoli, D. W. Dubois, B. D. San Filippo, and I. G. Kavouras., 2014: Air Pollution and Hospital Emergency Room and Admissions for Cardiovascular and Respiratory Diseases in Doña Ana County, New Mexico. *Environmental Research*, **129**, 39-46.

45 Thoma, M., 2013: http://martin-thoma.com/zero-mean-normalized-cross-correlation/. (last viewed 20151207).

46 Wallace, J.M. and Hobbs, P.V., 2006: Atmospheric science: an introductory survey **92**. *Academic Press*, Amsterdam.

47 Wang X., Z. Dong, J. Zhang, L. Liu, 2004: Modern dust storms in China: an overview. *Journal of Arid Environments*, **58**, 4, 559-574.

48 Wigner, K. A., and R. E., Peterson, 1987: Synoptic climatology of blowing dust on the Texas South Plains, 1947-84. *Journal of Arid Environments*. **13**, 199-209.

49 Yarnal, B., 1993: Synoptic Climatology in Environmental Analysis. Studies in Climatology Series. *Belhaven Press*, London.

50 Zhao L., and S. Zhao, 2006: Diagnosis and simulation of a rapidly developing cyclone related to a severe dust storm in East Asia. *Global and Planetary Change*, **52**, 1–4, 105-120.